Radar Probabilistic Data Association Filter with GPS Aiding for Target Selection and Relative Position Determination

by

Tyler P. Sherer

A thesis submitted to the Graduate Faculty of
Auburn University
in partial fulfillment of the
requirements for the Degree of
Master of Science

Auburn, Alabama
May 6, 2017

Keywords: GPS, Radar, RTK, Target Selection, PDAF

Approved by

David Bevly, Chair, Professor of Mechanical Engineering
George Flowers, Professor of Mechanical Engineering
John Hung, Professor of Electrical and Computer Engineering

Abstract

In this thesis, Global Positioning System (GPS) and radar measurements are utilized in a multi-sensor architecture to achieve a confident relative positioning solution between two vehicles. A GPS solution providing a three-dimensional positioning vector is determined using pseudorange and carrier phase measurements. The carrier phase measurements make sub-meter level accuracy achievable. However, the carrier phase ambiguity must be resolved before estimating the relative position vector. A Dynamic Base Real-Time Kinematic (DRTK) positioning algorithm using differential GPS methods is used to achieve highly precise relative positioning between the two GPS antennas. A comparison of the performance of the DRTK algorithm using either single frequency (L1 or L2 frequency only) or dual frequency (L1 and L2 frequency) measurements is introduced.

The radar measurements including range, range rate, and bearing are utilized in a probabilistic data association filter (PDAF). The PDAF determines which of the radar channels' solutions are considered valid, and the weighted mean of these solutions is used as the selected target measurements. The PDAF algorithm is discussed in great detail, and the performance of the PDAF algorithm using radar measurements and the performance of the DRTK solution are compared and presented demonstrating that the radar PDAF solution tracks the desired target with reasonable accuracy as long as the lead vehicle is in line of sight.

Finally, the DRTK algorithm is extended to incorporate the radar PDAF solution to increase solution availability, output rate, and reliability of the algorithm's solution. The PDAF algorithm's solution using the radar measurements can be utilized during GPS outages. The update rate of the radar measurements is ten times faster than the rate of the GPS receiver. The resultant combined system produces estimates at a much higher output rate.

The integrated DRTK/PDAF system is implemented with three integration architectures including two "switch" methods and a sensor fusion Kalman filter. Analysis of the accuracy of the integrated systems is presented using experimental data collected on various test vehicles, and some conclusions can be made. The GPS measurements can assist the PDAF solution when the lead vehicle is not visible to the following vehicle. Also, the DRTK/PDAF integrated system produces a more robust relative positioning solution at a higher update rate than either sensor could produce individually.

Acknowledgments

To begin, I would like to thank my Lord and Savior Jesus Christ for the work that He did on the cross that has been the focus of my life and the reason that I strive to glorify Him in all that I do. God is the one that has ultimately given me this opportunity and the ability to succeed. I give Him all the credit and praise for His provision.

Next, I would like to thank my family for all the support they have given me throughout life and especially these past couple of years. Thank you all for the examples of hard work and perseverance you have been to me. Dad, you are the greatest example of a godly man any son could ask for. Mom, you are the greatest encourager this world has ever seen. Both of your support and love has made this work in graduate school so much easier and much more enjoyable. Thank you. Thomas, you have been such a great example of a hard working man and engineer. Thank you for your encouragement and help. Amanda, you have encouraged me all through school. I am thankful for the time I had with you in Auburn.

I would also like to thank my friends, current and past, who have encouraged me along the way and challenged me to stay diligent in my work and in all that I do.

I would also like to thank Dr. Bevly for giving me the opportunity to work in his lab as a research assistant. I feel privileged to have gone to graduate school at Auburn University and to have worked in the GAVLAB. I would also like to thank Scott Martin for his willingness to help me with many different problems throughout graduate school especially at the beginning as I was getting started. Also, I would like to thank Grant Apperson for his help with data collection and his helpful input and ideas. To all the members of the GPS and Vehicle Dynamics Lab, thank you for the help many of you provided me during my time in the lab and all of the ping pong games that we played. Must of been thousands of them! War Eagle!

Table of Contents

List of Figures

List of Tables

Chapter 1

Introduction

1.1 Background and Motivation

The United States Air Force designed a system that could provide the location of a user anywhere in the world in the 1970s. A few years later, 24 NAVSTAR satellites were orbiting the earth in six orbital planes to ensure that at least four satellites were visible from a certain point on the earth's surface. The intended use for the Global Positioning System (GPS) was air and sea navigation. Both air and sea travel would ensure good sky visibility. However, during ground vehicle navigation, it can be difficult to acquire good sky visibility around trees and tall buildings, and because GPS requires four satellites to determine position, the system is limited. Due to this limitation, more satellites have been launched to bring the total number of satellites to 32 in the constellation. The accuracy of a standalone GPS solution is within a couple meters which is sufficient for some applications, but other applications require a much more precise determination of position. There are several sources of error that degrade the GPS signal and make it difficult to acquire the desired level of precision. Most of the error comes from atmospheric effects on the signal as it travels through the ionosphere and troposphere. Methods involving differential techniques can be used to mitigate these common errors between the receivers if they are in close proximity to one another. Here, "close" is defined as approximately under ten kilometers. Differential techniques have come to be known as Differential GPS (DGPS).

Some applications require an even higher level of precision than DGPS for positioning. A technique called Real-Time Kinematic (RTK) positioning can be used in these instances. This method utilizes the carrier phase measurement of the GPS signal, which beforehand was not used. Using the carrier phase for positioning can result in centimeter-level positioning.

However, in order to use the carrier phase, the whole number of cycles from the receiver to the satellite of the carrier phase measurement must be determined. This unknown value is called the integer ambiguity. A Kalman filter can be used to calculate floating point approximate estimates of the ambiguities, but the ambiguities must be integers which are more difficult to determine. In order to solve for the integer ambiguities, the LAMBDA method was created by Peter Teunnisen and other researchers at Delft University. Once the ambiguities are determined and assuming the receiver does not lose lock with the satellites, a position solution with accuracy of approximately one or two centimeters can be maintained. A static base station is required for RTK to ensure accurate global positioning. In this thesis, relative positioning is more important than global positioning; therefore, the algorithm calculates the relative position between the two receivers using the Dynamic Base RTK (DRTK) method. This method is most suitable for scenarios that are more concerned with relative positioning than global positioning with fixed or moving baselines.

As navigation systems are being developed, it is apparent that accurate and precise positioning is an imperative for both military and civilian ground vehicle guidance. A desire for autonomous vehicle control and navigation has become evident in the research and academic world. Advancements in this area such as precise spacing systems and collision avoidance systems would increase safety and increase fuel economy for vehicles traveling in a convoy. Convoy technology is needed whether the system is simply updating the drivers of the spacing between the vehicles or whether the system is functioning completely autonomously in Adaptive Cruise Control (ACC) or coordinated ACC using vehicle to vehicle (V2V) communication. In either of these cases, the ability of the relative position solution to be consistently precise in tight spacing is extremely important to ensure the safety of everyone on the road. Current systems employ radar or lidar sensors to measure range and range rate between vehicles. Radar, or radio detection and ranging, is often used to determine distance and speed of vehicles relative to the user. A radar system utilized in this work will be discussed in Chapter 3. For further information on the background of radar, see [10].

However, many of these current systems require extremely expensive sensors in order to ensure a stable solution often making them impractical for commercial use. Therefore, there is a significant desire for a cost-effective navigation system that civilians can afford. As the need for this technology increases, navigation systems incorporating multiple sensors have been developed and relied upon in many navigation situations. The work in this thesis will investigate methods of utilizing both the GPS signal and radar measurements in a single multi-sensor architecture for robust relative positioning. The cost-effectiveness of the navigation system is one of the most important parameters considered in this work. One of the main goals of this work is to develop and implement a robust relative positioning system that is also inexpensive and easily implemented.

1.2 Prior Work

This thesis involves integrating GPS and radar measurements to calculate relative positioning data for navigation of a following vehicle in a convoy scenario. The relative GPS positioning is performed using the differenced carrier phase measurements. This measurement and process will be described in further detail in Chapter 2. In 1985, the first use of the carrier phase measurements in a dynamic scenario occurred [19]. The carrier phase measurements include an innate ambiguity that must be resolved. This ambiguity is easily solved for as a floating point value, but it is important to fix the ambiguities into integers which will result in increased accuracy. The Least Squares Ambiguity Decorrelation Adjustment or LAMBDA method was developed by Delft University researchers in the 1990s shown in [24].

There is considerable work in the literature for the process of target selection for ground vehicles using radars. Different algorithms using the range, bearing, and range rate outputs of the radar can be found in [5] and [21] including the base algorithm that is used in this work which will be described in detail in Chapter 3. Also, much work has been done in the study of multi-vehicle target selection in Adaptive Cruise Control (ACC) applications [16].

There have also been considerable efforts in the area of multi-sensor fusion involving GPS and other sensors in order to acquire accurate relative positioning information. The work done in [14] describes a closely coupled GPS/INS solution for relative positioning. Similarly, the work in [4] describes the fusion of GPS and Ultra-wideband radios for carrier phase ambiguity resolution in RTK positioning. In the work explained in [22], a fusion system involving both radar and GPS measurements is developed for a marine navigation and anti-collision system. That work was applied entirely for marine navigation using Automatic Radar Plotting Aids (ARPA) and Automatic Identification System (AIS) which are commonly used in marine navigational systems. In contrast to this example, the carrier phase GPS and radar positioning algorithms detailed in this thesis are developed for ground vehicle applications. Also, the system implemented in this work utilizes low cost sensors, and the proposed fusion algorithm is a more straightforward integration of the GPS and radar measurements than the system seen in [22]. Furthermore, the radar measurements will be used to increase the update rate of the position solution and the GPS algorithms are formulated to utilize the L1 measurement or both the L1 and L2 measurements. The results for the single frequency and dual frequency solutions will be compared and shown in Chapter 2.

Autonomous following often relies on line of site to the lead vehicle due to the following vehicle using either vision with camera, lidar, radar, or a combination of the three [6]. These commonly used methods are exploited rather than GPS because of the occasional inconsistency and inaccuracy of standalone GPS measurements. However, GPS does allow for navigation in areas without clear line of sight, and the accuracy can be increased by utilizing the carrier phase relative position which will be shown later in this thesis.

1.3 Contributions

Though there have been many ways of incorporating multiple sensor measurements together to produce an accurate relative positioning solution, this thesis introduces a novel way

of integrating radar measurements with GPS positioning solutions. The major contributions to this field of research in this thesis are:

- Experimentally analyzing the drift in the radar's position solution when the lead vehicle is out of the radar's vision to show that the GPS position solution can be used to improve the position estimate
- Improving target identification and selection by integrating high precision differenced carrier phase measurements with the radar measurements
- Integrating range, range rate, and bearing measurements of a low cost radar with a GPS positioning solution to increase robustness and confidence in the navigation solution
- Testing the effects of multiple vehicle configurations and environments to analyze the performance of the integrated GPS/Radar algorithm

1.4 Thesis Outline

To begin, this thesis discusses the GPS signal structure and the errors that are intrinsic to it. Then, various differential positioning methods are described including the techniques to mitigate the common errors between GPS receivers. These techniques are compared, as well as visualized through experimental results in order to compare the accuracy of each method. The differential positioning algorithms are discussed in greater detail along with the derivation of how the relative position vector is determined.

Next, the basic radar measurements are discussed in Chapter 3 along with the channel architecture of the specific radar used in this work. The problem of target selection for radar tracking is discussed along with many issues that complicate the problem. A tracking algorithm for the radar is described in great detail. Experimental results are then shown displaying the algorithms tracking performance.

The GPS positioning solution is integrated with the radar in a multi-sensor fusion architecture, and experimental results are shown in Chapter 4. Finally, conclusions on the system's performance are also discussed along with some potential future works in this area of research in Chapter 5.

Chapter 2

Basics of GPS Navigation and Differential Positioning Techniques

2.1 GPS Signal

Before commercial navigation utilized it, the Global Positioning System (GPS) was developed as a satellite based navigation system for the military. It was designed to provide accurate positions, velocities, and time (PVT) for any user on the planet. Initially, there were 24 satellites or space vehicles (SVs) in varying orbit planes. Now, the total number of SVs has grown to 32. Each space vehicle broadcast signals on various L band carrier frequencies. The main two frequencies are the L1 and L2 signals. The L1 signal has a center frequency of 1575.42 MHz, and the L2 signal's center frequency is 1227.60 MHz. The L5 carrier frequency was introduced in March of 2009 and has a center frequency of 1176.45 MHz. The L5 signal is utilized in some systems, but currently, the primary signals used are the L1 and L2 signals.

The broadcast GPS signals are generated with several codes modulated onto their carrier signals. This specific form of modulation is known as binary phase shift keying (BPSK). Each period ranging code modulated onto the carrier signal is unique to each space vehicle. The codes are binary sequences known as pseudo-random noise (PRN) sequences. Any in-phase copy of the PRN codes have a high auto-correlation with itself but not with any other SV. The PRN codes have unique numbers for each of the satellites ranging from 1-32. For further details on the history of satellite constellations and the chosen architecture, see [15]. There are two parts of the code signal. The first is known as the C/A code (Coarse/Acquisition) which is accessible for civilian use and is another name for the PRN code. The other code is specifically designed for military use only and called precision codes or P(Y) code (also known as "Protected code" because it is encrypted).

Every C/A code is a unique sequence comprised of 1023 bits, also called chips which repeat every millisecond. Each C/A code chip has a duration of about 1 microsecond. The chipping rate, the rate of the C/A code chips, is 1.023 MHz (or megachips/second). The coarse/acquisition code is properly named because it is coarse compared to the precision codes. The P code is a unique section of a very long (on the order of 10^4 chips) PRN sequence. The chipping rate is 10.23 MHz which is ten times the chipping rate of the C/A code. The P-codes repeat once a week. Without the encryption key, there is not much use for the P(Y) code. Although, some "codeless" techniques have been developed to allow civilians to track the P(Y) carrier phase without the key.

A third component of the GPS signal is the navigation message. The navigation message is a binary-coded message composed of data including the health status of the satellite, ephemeris (satellite orbit information), clock bias parameters, and almanac data on the satellites. The navigation message bit has a duration of about twenty milliseconds and is transmitted at 50 bits per second. The entire navigation message frame, which contains the satellite ephemeris, clock parameters, and a $\frac{1}{25}^{th}$ of the almanac is broadcast every thirty seconds. The almanac data, because it contains so much data, is spread over 25 frames and takes 12.5 minutes for the entire message to be received.

The receiver's position is calculated by multiplying the time-of-flight of the signal from the satellite to the receiver by the speed of light resulting in the estimated range between that specific satellite and the receiver. The time-of-flight is found by subtracting the signal's time of arrival by the transmit time of the signal. The position of the receiver is then calculated then using a trilateration method. However, a GPS receiver requires a minimum of four satellite signals to estimate its position. Four satellites are necessary because the receiver's clock bias (i.e. clock receiver time relative to satellite time) is nonzero and must be estimated along with the receiver's position in the x, y, and z directions on Earth. The receiver's clock is not perfectly synchronized with the satellites, which results in an offset in the receiver clock. The offset is referred to here as a clock bias.

2.1.1 GPS Errors

Many different sources of error degrade the GPS signal which results in inaccurate range measurements. The receiver estimates the distance that the GPS signal traveled from the satellite, but this is not the actual range. This range estimate is known as the pseudorange, which contains many errors. Some of the major errors are included in the following: atmospheric errors that occur as the GPS signal passes through the ionosphere and troposphere, receiver and satellite clock errors, multipath errors occurring when the signal bounces buildings, attenuation as the signal passes through trees, and ephemeris errors.

The largest effect of these errors is due to the degradation of the signal that occurs as it propagates through the ionosphere and troposphere. The magnitude of this error is dependent on the elevation of the particular satellite because the more atmosphere the signal travels through between the satellite and the receiver, the greater the error. Therefore, the GPS signals from lower elevation SVs will travel through more atmosphere than a signal coming from a SV near the zenith.

The ionosphere is a region of ionized gases that are caused by the sun's radiation, and the ionosphere's state is determined predominately by the solar activity in the atmosphere. The ionized gases in the ionosphere cause a phase advance on the carrier signal which extends the pseudorange. The advance is directly proportional to the number of electrons the signal passes through. A group delay is also produced on the data modulated onto the carrier signal. The ionosphere activity widely varies depending on whether it is day or night, season of the year, and the solar activity for that specific region and time. Many different models have been formulated over the years to estimate the effects of the ionosphere on the signal in specific conditions.

The troposphere is a lower part of Earth's atmosphere. Tropospheric errors are caused by the refraction of the signal induced by the humidity in the troposphere. The propagation

speed of GPS signals in the troposphere is lower than in free space. Therefore, the pseudorange to the satellite appears longer. Most of the ionosphere delays can be mitigated using a dual-frequency receiver as seen in the work done in [12].

Another source of error in the GPS signal is the noise, bias, and drift in the SV's clock transmitted to the receiver. Whether the clock is fast or slow will determine whether the pseudorange is shorter or longer than the true range. The navigation data contains clock correction data that can be used to reduce these errors. The GPS receivers also possess their own clock errors that affect the pseudoranges, which must be estimated along with the receiver's position.

Multipath errors are another form of error in the GPS signal. These errors occur when the signal reflects off of nearby objects such as buildings or trees. Therefore, multipath errors are most commonly experienced in cities next to tall buildings. Because the signal must travel a longer path to the receiver, multipath errors increase the pseudorange the receiver estimates. The magnitude of the error can range from a few centimeters to several meters.

There can also be errors in the ephemeris data provided by the satellites which result in errors in the calculated satellite positions. Ground observation stations around the world monitor and estimate the trajectories of the satellites. These estimates are produced at the ground stations and sent to the satellites which are then transmitted down in the ephemeris data. Estimates of the SV positions and velocities in the near future are possible because of this process. The ephemeris data is refreshed every two hours at the ground stations. So, the errors induced by the ephemeris data will increase with time following the last ephemeris update.

A typical error budget for the GPS signal is shown in Table 2.1 and found in [18]. The user equivalent range error (UERE) is usually about 1% of the signal's wavelength as shown in [15]. The carrier signal's wavelength on the L1 frequency is about 19.03 centimeters which results in an error of roughly 2 millimeters. The wavelength of the code is much larger

at 293.1 meters which results in an error of 2.93 meters. The are pseudorange differential techniques, but because the error in the carrier is significantly smaller than the code error, the differential techniques that take advantage of the carrier signal can result in much more accurate solutions. These differential techniques incorporating the code and carrier are discussed in further detail later in this chapter. The atmosphere has a much greater effect on the L1 signal than the L2 signal because the L1 signal has a higher frequency. To determine the approximate position accuracy that the user can expect, the UERE must be multiplied by the dilution of precision (DOP). The DOP is a unitless parameter that provides a simple characterization of the satellite geometry relative to the user. Further discussion of the DOP can be found in Appendix A along with some further detail regarding GPS timing.

Table 2.1: GPS Error Model and User Equivalent Range Error (UERE) [18]

Error Source	C/A Range Error (m)	P(Y) Range Error (m)
Ephemeris data	2.1	2.1
Satellite Clock	2.1	2.1
Ionosphere	4.0	1.2
Troposphere	0.7	0.7
Multipath	1.4	1.4
Receiver measurement	0.5	0.5
UERE	5.3	3.6

2.1.2 GPS Measurements

As stated previously, GPS provides two types of measurements. These measurements are known as the code phase and carrier phase measurements. In order to visualize the errors involved in these measurements and how they are mitigated through differencing, Equation (2.1) and Equation (2.2) are shown below.

$$\rho = r + c(\delta t_r - \delta t^s) + I + T + M + \epsilon_\rho \tag{2.1}$$

$$\phi = r + c(\delta t_r - \delta t^s) - I + T + \lambda N + M + \epsilon_\phi \tag{2.2}$$

The code phase measurement is also referred to as the pseudorange, ρ, which was mentioned earlier in this chapter. The carrier phase measurement is designated as ϕ. For further information and for the derivation of these equations, see [15]. Each of these equations represent the pseudorange and carrier phase measurements between the receiver and a specific satellite in the constellation.

The true range between the satellite and each receiver is denoted by r in Equations (2.1-2.2). δt_r and δt^s denote the receiver clock error and the satellite clock error, respectively which are multiplied by the speed of light, c. Ionosphere errors, I, and troposphere errors, T, are also accounted for in this formulation. M denotes the multipath error that affects the signal. ϵ represents the random noise on both signals. The random noise on the carrier phase measurement is 1% as mentioned previously and therefore much smaller than that on the pseduorange measurement as shown in Equations (2.1-2.2). The wavelength, λ, of the L1 signal is approximately 19.03 centimeters, and the L2 signal's wavelength is approximately 24.42 centimeters. The integer ambiguity is denoted as N and is the unknown number of cycles between the receiver and satellite that when resolved correctly allows for highly accurate solutions in carrier phase positioning. The pseudorange and carrier phase measurements are both in units of meters.

2.2 Differential GPS Positioning Techniques

About a decade after the launch of the Global Positioning System, many differential positioning techniques were formulated to help mitigate common errors between GPS receivers that were in close proximity to one another. Around 10 kilometers or less has been considered close proximity for these applications. If the two receivers are close enough to one another, the atmospheric effects on each receiver's incoming signals will be very similar. Likewise, the satellite clock and ephemeris errors of the two receivers are identical. Therefore, close proximity is vital when performing differential techniques. Otherwise, the assumption that these errors are similar or identical between receivers will be incorrect and cause decreasing

accuracy in solutions. Not all errors are mitigated using differential techniques. Errors such as multipath and receiver clock errors are not common between receivers and must still be accounted for. With multiple receivers, a user can difference measurements between the receivers and eliminate a significant amount of the errors inherent to the signal. This allows for a more accurate relative positioning solution between users.

Several types of differential positioning methods are accessible, including Wide Area Augmentation System (WAAS), Satellite Based Augmentation System (SBAS), a Ground Based Augmentation System (GBAS), Differential GPS (DGPS), and Real-Time Kinematic (RTK) positioning.

The SBAS uses thoroughly surveyed base stations around the world to upload ephemeris, clock, and atmospheric corrections to geostationary (GEO) satellites, which then relay the information to the user. These GEO satellites are separate from GPS SVs. The WAAS is a type of SBAS and was declared operational by the Federal Aviation Administration (FAA) in 2003. The WAAS is accessible to civilians and broadcasts corrections used in North America from geostationary satellites in the form of navigation messages modulated on GPS-like signals on the L1 frequency. The expected position accuracy of the WAAS solution is less than ten meters. Higher accuracy may be expected from the GBAS solution because the GBAS local ground stations have better corrections that more closely correlate with the errors of that specific region.

The RTK method was initially designed for surveying but has found many various applications in recent years. In the RTK method, the measurements of the reference receiver are transmitted to the rover over a radio link, and because the RTK technique uses the carrier phase with a smaller UERE than the pseudorange, a higher accuracy of position and velocity can be obtained. However, when incorporating the carrier phase, the process becomes more complicated. This complication comes from the necessity to resolve the integer ambiguities which are defined as the number of integer cycles in the carrier phase between the receiver and every satellite (while the receiver has maintained a lock on the GPS carrier signal). If these

integer ambiguities are successfully resolved, an extremely accurate solution of millimeter level can be found. The RTK method assumes that the reference station (base) is static, and the position of the base is well known. A version of RTK that has been developed for scenarios of leader-follower configurations where both the rover and the base are moving is known as Dynamic Base RTK (DRTK) positioning and is discussed later in this thesis.

2.3 Real-Time Kinematic (RTK) Positioning

In order to make surveys more efficient, the RTK mode was created to compute positions of a rover receiver in real time. The RTK method requires the ability to calculate the integer ambiguities while the rover is in motion. This is also known as *on-the-fly* (OTF) *initialization*, which is accomplished in real time. The performance of an RTK system is measured based on the initialization time and the accuracy of the solution. Because of their highly accurate results, RTK solutions are often used as references to compare the accuracy of other navigation systems.

The biggest challenge when performing carrier phase positioning is resolving the unknown number of cycles between the receiver and every satellite, also known as integer ambiguities. The ambiguities remain constant as long as the receiver maintains a lock on the satellite signals. The ambiguities will be integers because the receiver measures the fraction of the carrier signal's phase. The ambiguities are usually denoted by N. With a single GPS receiver, resolving ambiguities can be difficult and requires long periods of surveyed static data to solve for them correctly. As stated before, when using two receivers in close proximity, many common errors between the two receivers can be mitigated by taking the difference of the observations from each receiver. Techniques such as Differential GPS (DGPS) use a method of broadcasting measurements from one receiver to another over radio link such that the user can mitigate the common errors between the two receivers. RTK positioning techniques use these same receiver-linking methods and entails a well-surveyed ground base station. The ground base station has a very well known global location, which

is usually determined by taking a static data set of 24 hours or more. Then, the radio link is setup between the base and the rover, and the base transmits observations to the rover. The observations transmitted include single and double differenced measurements to mitigate the common errors between the receivers, and a Kalman filter is used to initially estimate the floating point ambiguities. The LAMBDA method is then used to fix the estimated integer ambiguities, and a least squares method is used to estimate the relative position vector (RPV) between the two receivers.

2.4 Dynamic Base Real-Time Kinematic (DRTK) Positioning

One of the key characteristics of traditional RTK positioning is the requirement of a static base station with a well known global position. In applications with a moving base station receiver, the Dynamic Base RTK (DRTK) system can be utilized. Because of the dynamic nature of the base station, the global position accuracy is lost. However, the relative positioning between the two receivers retains the RTK method's centimeter-level accuracy. The DRTK technique operates similarly to the RTK method in mitigating the common mode errors between the two receivers by differencing the measurements allowing for the determination of a highly accurate RPV between the receivers. Similar to RTK positioning, there are three stages in the DRTK algorithm. The first stage is estimation of the floating point or decimal values of the carrier phase ambiguities using a Kalman filter. Secondly, the LAMBDA method is used to determine the fixed integer ambiguities. Lastly, the fixed integer ambiguities are subtracted from the carrier phase measurements, and using least squares estimation, the RPV between the two receivers can be determined. The DRTK algorithm is discussed in further detail in this chapter, and other examples of DRTK applications and implementations can also be seen in [9], [14], and [25].

2.5 Differenced Observation Measurements

This section discusses single differenced and double differenced observation measurements and how differencing Equations (2.1) and (2.2) between two GPS receivers with the same time-epochs allows for the mitigation of the common mode errors shared between the receivers.

2.5.1 Single Differenced Observation Measurements

As mentioned previously in this chapter, atmospheric errors can be mitigated when the pseudorange and carrier phase measurements of two receivers are differenced assuming the receivers are within close proximity to one another. This may not always be the case such as when strange weather occurs or during times of high solar radiation activity in the atmosphere, but for the most part, this is a good assumption. The single differenced pseudorange and carrier phase formulations are shown below in Equations (2.3-2.4)

$$\Delta\rho_{r_1-r_2} = \rho_{r_1-r_2} + c\delta t_{r_1-r_2} + \epsilon_{\rho_{r_1-r_2}} \tag{2.3}$$

$$\Delta\phi_{r_1-r_2} = \phi_{r_1-r_2} + c\delta t_{r_1-r_2} + \lambda N_{r_1-r_2} + \epsilon_{\phi_{r_1-r_2}} \tag{2.4}$$

where Δ designates the single differenced operation between receiver 1, r_1, and receiver 2, r_2. It is assumed also that the multipath errors are negligible in this technique.

This formulation allows for the mitigation of the atmospheric errors and the satellite clock errors. However, the receiver clock errors still remain. The integer ambiguity now represents a relative, or differenced, integer ambiguity between the two receivers.

2.5.2 Double Differenced Observation Measurements

Although the single difference operation helps to eliminate atmospheric errors, satellite clock errors, and multipath errors, there is still receiver clock errors that remain in Equations (2.3-2.4). In order to mitigate the residual clock errors, a second differencing operation can

be used. While the single differenced values were the differenced measurements between two receivers, the double differenced measurements are the differences of the single differenced measurements to a specific satellite. This particular satellite is determined as the SV that will give the most reliable measurements and is known as the base satellite (usually the satellite at the highest elevation). The base satellite's single differenced measurements are subtracted from all the other satellites' single differenced measurements. This differencing results in the double differenced measurements that no longer include the receiver clock biases. The double differenced measurements formulation is shown below in Equations (2.5) and (2.6)

$$\nabla\Delta\rho_{r_1-r_2}^{s_1-s_2} = \rho_{r_1-r_2}^{s_1-s_2} + \epsilon_{\rho_{r_1-r_2}}^{s_1-s_2} \tag{2.5}$$

$$\nabla\Delta\phi_{r_1-r_2}^{s_1-s_2} = \phi_{r_1-r_2}^{s_1-s_2} + \lambda N_{r_1-r_2}^{s_1-s_2} + \epsilon_{\phi_{r_1-r_2}}^{s_1-s_2} \tag{2.6}$$

where s_1 and s_2 are a regular satellite and the base satellite, respectively. The equations formulated above are now in terms of relative position and relative residual noise measurements between the two receivers. Note that residual noise in the measurements will increase with both the single difference operation and double difference operation because the residual noise is random and not common to both of the receivers.

2.6 Kalman Filter Floating Point Ambiguity Estimation

As stated previously in this chapter, the carrier phase ambiguities are initially estimated as floating point or decimal values using a Kalman filter. The state vector used in the Kalman filter is shown below in Equation (2.7)

$$x = \left[N_{r_1-r_{2L1}}^{1} \cdots N_{r_1-r_{2L1}}^{m} \; N_{r_1-r_{2L2}}^{1} \cdots N_{r_1-r_{2L2}}^{m} \right]^T \tag{2.7}$$

where m is the number of satellites. This configuration allows for the estimates of single differenced ambiguities on both the L1 and L2 frequencies assuming dual frequency measurements are available. Therefore, the state vector, x, is a column vector that is twice the length of the number of satellites being used. In a single-frequency configuration (i.e. L1 measurements only), the state vector would be of length m.

2.6.1 Measurement Model

The required configuration of the measurement model for the Kalman filter is of the form $z = Hx$. Although this is not a trivial task, it is possible to obtain this form by combining Equations (2.3) and (2.4). The single differenced pseudorange and carrier phase measurements are a function of two unknown terms and the stochastic noise term. The combination is rewritten in matrix form and shown in Equation (2.8) below.

$$\begin{bmatrix} \Delta\rho^s_{r_1-r_2} \\ \Delta\phi^s_{r_1-r_2} \end{bmatrix} = \begin{bmatrix} u^s_{r_{1_x}} & u^s_{r_{1_y}} & u^s_{r_{1_z}} & 1 \\ u^s_{r_{1_x}} & u^s_{r_{1_y}} & u^s_{r_{1_z}} & 1 \end{bmatrix} \begin{bmatrix} r^s_{r_{1_x}-r_{2_x}} \\ r^s_{r_{1_y}-r_{2_y}} \\ r^s_{r_{1_z}-r_{2_z}} \\ c\delta t_{r_1-r_2} \end{bmatrix} + \begin{bmatrix} 0 \\ \lambda \end{bmatrix} N^s_{r_1-r_2} \tag{2.8}$$

For further information, derivation, and application of the Kalman filter see [5]. The particular satellite in Equation (2.8) above, is denoted by superscript s, and $r_{r_1-r_2}$ designates the relative range term between the receivers composed of the x, y, and z components in the Earth-Centered Earth-Fixed (ECEF) coordinate frame. These relative range terms must be removed from the equation in order for the Kalman filter to estimate the ambiguities. The geometry matrix, G, is shown below in Equation (2.9) and consists of the unit vectors from the receiver to the satellite and a column of ones designating the clock bias terms.

$$G = \begin{bmatrix} u^{s_1}_{r_{1_x}} & u^{s_1}_{r_{1_y}} & u^{s_1}_{r_{1_z}} & 1 \\ \vdots & \vdots & \vdots & \vdots \\ u^{s_m}_{r_{1_x}} & u^{s_m}_{r_{1_y}} & u^{s_m}_{r_{1_z}} & 1 \end{bmatrix} \tag{2.9}$$

The derivation of the vector product of the RPV is shown below in Equation (2.10).

$$r^s_{r_1-r_2} = \begin{bmatrix} u^s_{r_{1_x}} & u^s_{r_{1_y}} & u^s_{r_{1_z}} \end{bmatrix} \begin{bmatrix} r^s_{1_x} \\ r^s_{1_y} \\ r^s_{1_z} \end{bmatrix} - \begin{bmatrix} u^s_{r_{2_x}} & u^s_{r_{2_y}} & u^s_{r_{2_z}} \end{bmatrix} \begin{bmatrix} r^s_{2_x} \\ r^s_{2_y} \\ r^s_{2_z} \end{bmatrix} \tag{2.10}$$

The distance from each of the receivers to a certain satellite is significantly larger than the distance from one receiver to the other. Therefore, the unit vectors to each satellite from receiver 2 can be assumed to be the same as the unit vectors from receiver 1 shown in Equation (2.11).

$$\begin{bmatrix} u^s_{r_{1_x}} & u^s_{r_{1_y}} & u^s_{r_{1_z}} \end{bmatrix} \approx \begin{bmatrix} u^s_{r_{2_x}} & u^s_{r_{2_y}} & u^s_{r_{2_z}} \end{bmatrix} \tag{2.11}$$

The derivation can now be redefined by Equation (2.12).

$$r^s_{r_1-r_2} = \begin{bmatrix} u^s_{r_{1_x}} & u^s_{r_{1_y}} & u^s_{r_{1_z}} \end{bmatrix} \begin{bmatrix} r^s_{r_{1_x}} - r^s_{r_{2_x}} \\ r^s_{r_{1_y}} - r^s_{r_{2_y}} \\ r^s_{r_{1_z}} - r^s_{r_{2_z}} \end{bmatrix} \tag{2.12}$$

The single differenced carrier phase ambiguity, $N^s_{r_1-r_2}$, in Equation (2.8) must be isolated from the single differenced pseudorange and carrier phase range observations in order for it to be estimated. To accomplish this, each term in the Equation (2.8) matrix must be multiplied by the left null space of the geometry matrix. The left null space, L, is defined such that $L^T G = 0$ and is shown below in Equation (2.13).

$$L = leftnull \left(\begin{bmatrix} u_{r_{1_x}}^{1\cdots m^T} & u_{r_{1_y}}^{1\cdots m^T} & u_{r_{1_z}}^{1\cdots m^T} & 1 \\ u_{r_{1_x}}^{1\cdots m^T} & u_{r_{1_y}}^{1\cdots m^T} & u_{r_{1_z}}^{1\cdots m^T} & 1 \\ u_{r_{1_x}}^{1\cdots m^T} & u_{r_{1_y}}^{1\cdots m^T} & u_{r_{1_z}}^{1\cdots m^T} & 1 \\ u_{r_{1_x}}^{1\cdots m^T} & u_{r_{1_y}}^{1\cdots m^T} & u_{r_{1_z}}^{1\cdots m^T} & 1 \end{bmatrix} \right) \tag{2.13}$$

When multiplying Equation (2.8) by Equation (2.13), the right hand side of the equation is removed. This results in a cleaner formulation.

The measurement vector in the Kalman filter measurement model is denoted as z and contains the single differenced pseduorange and carrier phase measurements. This vector stays on the left hand side of the measurement equation and is multiplied by L and can be seen below in Equation (2.14).

$$z = L \begin{bmatrix} \Delta\rho_{r_1-r_{2L1}}^{1\ldots m} & \Delta\rho_{r_1-r_{2L2}}^{1\ldots m} & \Delta\phi_{r_1-r_{2L1}}^{1\ldots m} & \Delta\phi_{r_1-r_{2L2}}^{1\ldots m} \end{bmatrix}^T \tag{2.14}$$

The measurement vector shows the single differenced measurements for satellites 1 to m on the L1 and L2 frequencies. The coefficient matrix for the state vector, x, in the Kalman filter measurement model is denoted by H and is shown below in Equation (2.15)

$$H = L \begin{bmatrix} 0_{2mxm} & 0_{2mxm} \\ \lambda_{L1} I_{mxm} & 0_{mxm} \\ 0_{mxm} & \lambda_{L2} I_{mxm} \end{bmatrix} \tag{2.15}$$

where λ_{L1} and λ_{L2} represent the wavelengths for the L1 and L2 frequencies, respectively.

The measurement model now matches the $z = Hx$ form of the Kalman filter. Next, the Kalman filter measurement update is implemented as shown in Equations (2.16-2.18) below.

$$K_k = P_k^- H_k^T (H_k P_k^- H_k^T + R_k)^{-1} \tag{2.16}$$

$$P_k^+ = (I - K_k H_k) P_k^- \tag{2.17}$$

$$\hat{x}_k^+ = \hat{x}_k^- + K_k(z_k - H_k\hat{x}_k^-) \tag{2.18}$$

Here, K denotes the Kalman gain, P denotes the error covariance matrix, H is the measurement matrix, and R represents the measurement uncertainty matrix. The state vector and the error covariance matrix are updated using the Kalman gain, the measurement matrix, and the previous error covariance and estimates. The initialization of the error covariance matrix and state vector is discussed in a later section along with the measurement uncertainty calculation.

2.6.2 Propagation Model

The Kalman filter time update equations propagate the state estimates, x, and error covariance matrix, P. The equations describing the Kalman filter time update operation are shown below in Equations (2.19-2.20).

$$\hat{x}_{k+1}^- = \Phi_k\hat{x}_k^+ \tag{2.19}$$

$$P_{k+1}^- = \Phi_k P_k^+ \Phi_k^T + Q \tag{2.20}$$

The process noise matrix is denoted by Q and the discrete state transition matrix is represented by Φ. If the GPS receiver maintains a lock on the signal on a satellite between measurement epochs, the carrier phase ambiguity will remain constant. In this case, the state transition matrix would be the identity matrix with a size equal to the number of single differenced ambiguity estimates, and the process noise matrix would be equal to zero. However, in order to keep the error covariance from resulting in a zero gain matrix, Q is set to $1\text{x}10^{-6}$ times the identity matrix with equal dimensions to the number of single differenced ambiguity estimates.

2.6.3 Initializing and Implementing Filter

Initialization of the state vector, x, is done using single differenced pseudorange and carrier phase measurements from each satellite in view. The initial estimate of the single differenced ambiguities, shown below in Equation (2.21), is equal to the difference in the single differenced pseudorange and single differenced carrier phase measurement.

$$\hat{x} = \begin{bmatrix} (\Delta\rho^1_{r_1-r_2\,L1} - \Delta\phi^1_{r_1-r_2\,L1})/\lambda_{L1} \\ \vdots \\ (\Delta\rho^m_{r_1-r_2\,L1} - \Delta\phi^m_{r_1-r_2\,L1})/\lambda_{L1} \\ (\Delta\rho^1_{r_1-r_2\,L2} - \Delta\phi^1_{r_1-r_2\,L2})/\lambda_{L2} \\ \vdots \\ (\Delta\rho^m_{r_1-r_2\,L2} - \Delta\phi^m_{r_1-r_2\,L2})/\lambda_{L2} \end{bmatrix} \tag{2.21}$$

The estimates are divided by the signal's wavelength, λ, to convert them into units of cycles.

The error covariance matrix, P, is initialized as $\frac{1}{2}$ times the identity matrix that is twice the size of the number of visible satellites or $2m$ x $2m$. The measurement uncertainty, R, is estimated after each measurement update based on the expected variance which is discussed in [18]. GPS observation measurement variance is a function of the characteristics of the receiver and the carrier to noise ratio, C/N_0, of the incoming signal. The anticipated pseudorange and carrier phase measurement variances are given by Equations (2.22-2.25).

$$\sigma^2_\rho = \sigma^2_{\rho_{atm}} + \sigma^2_{DLL} \tag{2.22}$$

$$\sigma_{DLL} = \lambda_C \sqrt{\frac{4d^2 B_{n\rho}}{C/N_0}\left(2(1-d) + \frac{4d}{TC/N_0}\right)} \tag{2.23}$$

$$\sigma^2_\phi = \sigma^2_{\phi_{atm}} + \sigma^2_{PLL} \tag{2.24}$$

$$\sigma_{PLL} = \frac{\lambda}{2\pi}\sqrt{\frac{B_{n\phi}}{C/N_0}\left(1 + \frac{1}{TC/N_0}\right)} \tag{2.25}$$

The values provided in Table 2.2 were used to calculate the above variances and are typical values of GPS receiver characteristics found in [12] and [13]. Equation (2.22) and Equation (2.24) show the calculation for the individual pseudorange and carrier phase measurement variances, respectively. However, it is a combination of the two measurements that are observables in the filter such that R, the measurement uncertainty matrix, is a function of the measurement noise on receiver 1 and receiver 2.

Table 2.2: Pseudorange and Carrier Phase Measurement Variance Parameters [12]

Parameter	Description	Value
$\sigma^2_{\rho_{atm}}$	Variance due to the atmospheric code delay	5.22 m
λ_C	Code Chip Spacing	293.05 m
d	Correlator Spacing	0.5 chips
$B_{n\rho}$	Code Loop Noise Bandwidth	2 Hz
T	Prediction Integration Time	5 ms
$\sigma^2_{\phi_{atm}}$	Variance due to the atmospheric carrier delay	0.03 m
λ_{L1}	Carrier Signal Wavelength on L1	19.03 cm
λ_{L2}	Carrier Signal Wavelength on L2	24.42 cm
$B_{n\phi}$	Carrier Loop Noise Bandwidth	18 Hz

Assumptions made at this point include that atmospheric errors have been eliminated in the single differencing of the measurements and that the measurements between receivers are uncorrelated. These assumptions result in a measurement uncertainty matrix, R, that is a diagonal matrix shown below in Equation (2.26).

$$R = \begin{bmatrix} \sigma^2_{r_{1\rho}} + \sigma^2_{r_{2\rho}} & 0 \\ 0 & \sigma^2_{r_{1\phi}} + \sigma^2_{r_{2\phi}} \end{bmatrix} \tag{2.26}$$

The above representation for R is for one satellite. The actual dimensions of R is twice the size of the number of visible satellites available.

Some modifications to the Kalman filter state vector and error covariance matrix dimensions do occur for a couple different reasons. The first modification is caused by changing satellite constellations. When a satellite that was being tracked by the receivers is lost, the

ambiguity estimate corresponding to that satellite is removed from the state vector. Likewise, the corresponding row and column of the error covariance matrix is also removed. If a new satellite comes into view (and is acquired by the receivers), an ambiguity estimate is added to the state vector and the corresponding row and column are added to the error covariance matrix. Initialization of the error covariance matrix and new ambiguity estimate is performed the same as before. Another reason for a modification is if a cycle slip occurs. A cycle slip happens when a receiver loses lock and reacquires lock with the same satellite in between measurement updates. This can be troublesome because the carrier phase ambiguity actually changes, which voids the previous estimate of the ambiguity because the ambiguity is assumed to be constant. This would corrupt the RPV solution significantly. Therefore, a cycle slip detection method is used with every new measurement before the update step. To compute a time differenced ambiguity estimate, the single differenced pseudorange and carrier phase measurements from the current and previous steps are used. This process is shown below in Equation (2.27).

$$\Delta N^s_{k,k-1} = [(\Delta\rho^s_k - \Delta\phi^s_k) - (\Delta\rho^s_{k-1} - \Delta\phi^s_{k-1})]/\lambda \tag{2.27}$$

A threshold for the cycle slip detection is compared with $\Delta N^s_{k,k-1}$. The threshold for this thesis was selected as one cycle. If $\Delta N^s_{k,k-1}$ exceeds the threshold, then the algorithm declares that the measurement experienced a cycle slip and the ambiguity estimate and covariance are reset as if a new satellite has come into view.

2.7 Fixed Integer Ambiguity Estimation using the LAMBDA Method

As stated previously, the carrier phase ambiguity estimates are still floating point values. Therefore, the second step of the RPV estimation is used to fix the ambiguity estimates into integers. A transformation matrix must first be created in order to transform the single differenced quantities into double differenced quantities. Recognizing that it is a linear

process, a transformation matrix must be formulated. An example of a transformation matrix for five common satellites is shown below in Equation (2.28).

$$C = \begin{bmatrix} 1 & 0 & -1 & 0 & 0 \\ 0 & 1 & -1 & 0 & 0 \\ 0 & 0 & -1 & 1 & 0 \\ 1 & 0 & -1 & 0 & 1 \end{bmatrix} \tag{2.28}$$

In this example, the third single differenced ambiguity estimate is selected as the base estimate. The base is subtracted from the other single differenced ambiguity estimates resulting in four double differenced ambiguities using Equation (2.29) below.

$$\hat{N}_{\nabla\Delta} = C\hat{N}_{\Delta} \tag{2.29}$$

The transformation matrix is also applied to the covariance matrix as seen in Equation (2.30).

$$P_{\hat{N}_{\nabla\Delta}} = CP_{\hat{N}_{\Delta}}C^T \tag{2.30}$$

The next step is to convert the floating point ambiguity estimates into fixed integer ambiguities. The most obvious method would be simply rounding the floating point values to integers. However, Kalman filter's estimates of the error covariance can aid in a more informed method. The Least Squares Ambiguity Decorrelation Adjustment or LAMBDA method method begins by decorrelating the ambiguity estimates in a transformation that results in a nearly diagonal error covariance matrix which is shown in [7]. This new covariance matrix is used to estimate the integer ambiguities beginning with the ambiguity estimate having the lowest variance. Once the integer ambiguities are estimated, the estimates are transformed back into the initial "coordinate" frame.

Even though the LAMBDA method is considered the most capable carrier phase ambiguity estimation technique, the method's solution is not always guaranteed to be correct

as seen in [11]. The most common way to determine the validity of the integer ambiguity estimate is the ratio test. The ratio test takes the ratio of the top two candidates for the integer ambiguities, $\breve{N}_1$ and $\breve{N}_2$, compares their deviations to the initially estimated floating point carrier phase ambiguities, $\hat{N}$. The deviations, d, are shown in Equation (2.31).

$$d_i = (\hat{N} - \breve{N}_i)P_N^{-1}(\hat{N} - \breve{N}_i)^T \tag{2.31}$$

If the ratio, $\frac{d_1}{d_2}$, is above a determined threshold, the ratio test takes the top candidate as the correct integer ambiguity fix. The ratio threshold selected in this work for the ratio test was three based on the findings in [23].

2.8 Relative Position Vector Estimation using Least Squares

Estimating the RPV between the GPS receivers is the final step in the algorithm and can be performed now that the carrier phase integer ambiguities have been estimated. Note that the RPV is estimated whether the ratio test is passed or not. The RPV estimate is denoted as a high precision solution when the integer estimates are available or a low precision solution when the floating point estimate must be used. The RPV solution procedure is the same no matter the precision of the ambiguity estimates. The form of the RPV estimation algorithm is derived from Equation (2.6) and Equation (2.12) and shown below in Equation (2.32).

$$\nabla\Delta\phi_{r_1-r_2} - \lambda\nabla\Delta N_{r_1-r_2} = \Delta\bar{u}_{r_1}\bar{r}_{r_1-r_2} + \upsilon_{r_1-r_2} \tag{2.32}$$

It is important to note that the Δ in the $\Delta\bar{u}_{r_1}\bar{r}_{r_1-r_2}$ term designates that the base satellite unit vector has been subtracted out from the correct geometry matrix. Using the least squares method, the RPV between the two GPS receivers is estimated as shown in Equation (2.33).

$$\bar{r}_{r_1-r_2} = (\Delta\bar{u}_{r_1}^T\Delta\bar{u}_{r_1})^{-1}\Delta\bar{u}_{r_1}^T(\nabla\Delta\phi_{r_1-r_2} - \lambda\nabla\Delta N_{r_1-r_2}) \tag{2.33}$$

For further information and examples on least-squares estimation, see the work in [8].

2.9 Single Frequency Implementation

The algorithms discussed in the previous sections incorporated both the L1 and L2 frequency measurements. However, these techniques can also be performed using single frequency GPS receivers. One goal of this work is to utilize a single frequency DRTK algorithm and to analyze its performance compared to the dual frequency algorithm. Single frequency receivers and antennas are far cheaper than dual frequency hardware which can be a great advantage in low-budget applications.

The single frequency algorithm uses the same multi-step process as the dual frequency algorithm. The carrier phase ambiguities are estimated using the Kalman filter. However, modifications must be made to the state vector, the measurement vector, the measurement matrix, and the left null space matrix. These modification are made to only include the L1 information as seen in Equations (2.34 - 2.37).

$$x = \begin{bmatrix} N^{s_1}_{r_1-r_2 L_1} & \cdots & N^{s_m}_{r_1-r_2 L_1} \end{bmatrix}^T \tag{2.34}$$

$$z = L \begin{bmatrix} \Delta\rho^{s_1 \cdots s_m}_{r_1-r_2 L_1} & \Delta\phi^{s_1 \cdots s_m}_{r_1-r_2 L_1} \end{bmatrix}^T \tag{2.35}$$

$$H = L \begin{bmatrix} 0_{mxm} \\ \lambda_{L_1} I_{mxm} \end{bmatrix} \tag{2.36}$$

$$L = leftnull \left(\begin{bmatrix} u^{1\cdots m^T}_{r_{1_x}} & u^{1\cdots m^T}_{r_{1_y}} & u^{1\cdots m^T}_{r_{1_z}} & 1 \\ u^{1\cdots m^T}_{r_{1_x}} & u^{1\cdots m^T}_{r_{1_y}} & u^{1\cdots m^T}_{r_{1_z}} & 1 \end{bmatrix} \right) \tag{2.37}$$

Single frequency implementation can also be done using the L2 frequency carrier signal only.

The LAMBDA method is still used to find integer estimates of the double differenced carrier phase ambiguities, and least squares is used to estimate RPV. Because the number of

measurements has been reduced, the uncertainty in the ambiguity estimates increases, and the chance of successfully fixing integers decreases.

2.10 Experimentation and Results

In order to analyze the performance of the single frequency algorithm compared to the dual frequency algorithm, both static and dynamic GPS data was collected and processed using the method described above. For both data collections, two Novatel ProPak V3 GPS receivers were utilized. The static data set was collected using two GPS antennas attached to the roof of the Woltosz Engineering Research Laboratory at Auburn University. The two Novatel receivers were used previously to calculate RTK position solutions for each antenna on the roof as a fixed baseline reference. The receivers reported measurements at 2 Hz on both the L1 and L2 frequencies. Accuracy and availability of a high precision solution were the parameters by which the performance of the algorithms were evaluated.

Both the single frequency and dual frequency DRTK algorithms' accuracies were determined by comparing the estimates of the RPV to the difference in the RTK positions of the two receivers used as the reference. The low precision solution was calculated at every epoch. However, the high precision solution was only computed when three or more fixed integer ambiguity estimates were available. The first data set that analyzed both the low precision and high precision RPV is the static data set on the Woltosz Laboratory roof pictured in Figure 2.1. Note that the background mapping was provided by *GPS Visualizer*.

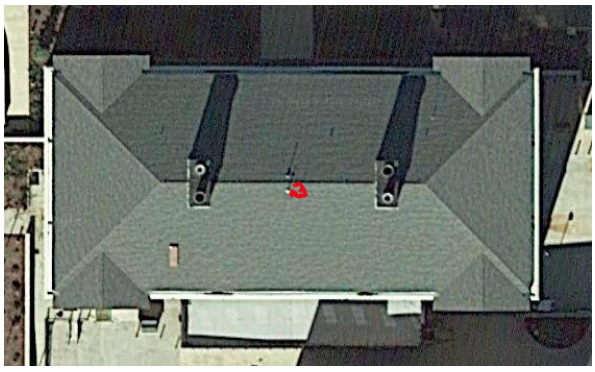

Figure 2.1: Novatel Reported Position for Woltosz Laboratory Roof Antenna

The antennas are spaced approximately 1.75 meters apart. The duration of the data collection was approximately ten minutes. The high precision baseline error versus time for both the single frequency and dual frequency DRTK algorithms can be seen in Figure 2.2.

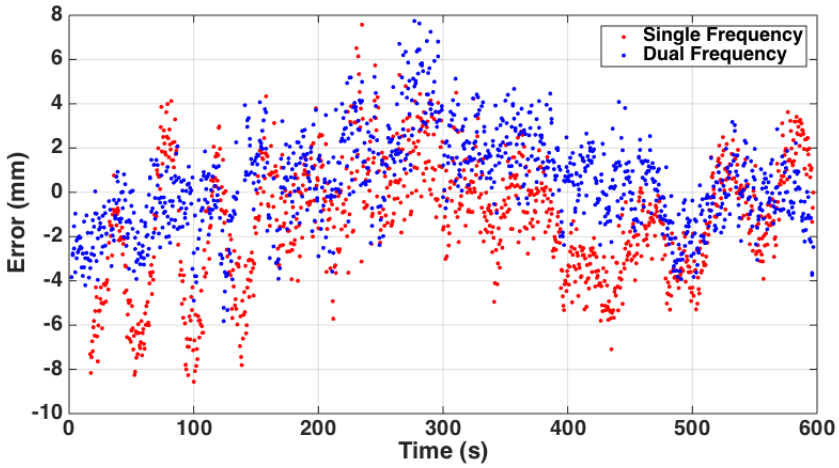

Figure 2.2: High Precision Baseline Error for a Static Data Set with Single and Dual Frequency Algorithms

It is clear that the errors between the single frequency and dual frequency solutions have similar magnitudes of error throughout the data set. The low precision baseline error for the single frequency and dual frequency algorithms is also provided in Figure 2.3. As seen

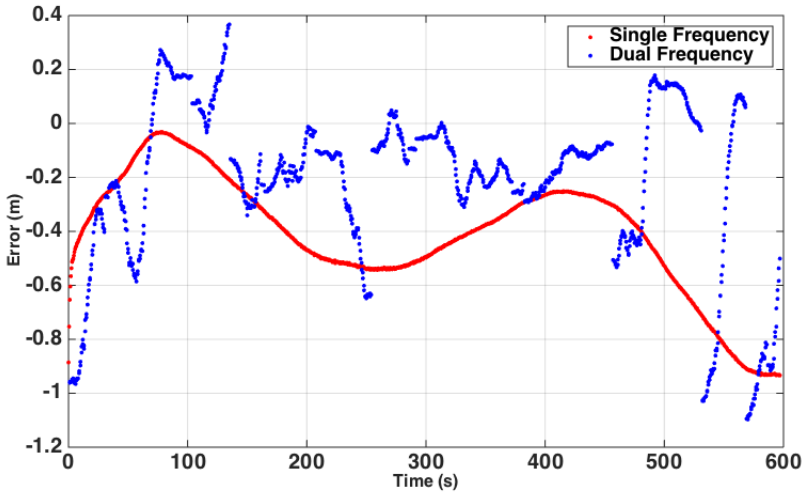

Figure 2.3: Low Precision Baseline Error for a Static Data Set with Single and Dual Frequency Algorithms

before in Figure 2.2, both the single frequency and dual frequency high precision solutions stay within one centimeter of the RTK reference solution for the duration of the data run. The maximum error for the low precision solutions is approximately one meter. Although this is not nearly as precise as the high precision solution, it is a great improvement from the standalone GPS solution whose error is occasionally several meters.

The standard deviations and variances for each of the solutions were calculated as well as the root mean squared error (RMSE) for each solution. All of these statistics can be seen in Table 2.3 and Table 2.4 where std and var are the standard deviation and variance, respectively.

Table 2.3: High Precision DRTK Solution Statistics for Static Data Set

	Dual Frequency	Single Frequency
std, σ (m)	0.00215	0.00273
var, σ^2 (m^2)	$4.62250e^{-5}$	$7.4529e^{-5}$
RSME (m)	0.00219	0.00288

Table 2.4: Low Precision DRTK Solution Statistics for Static Data Set

	Dual Frequency	Single Frequency
std, σ (m)	0.29853	0.22020
var, σ^2 (m^2)	0.08912	0.04848
RSME (m)	0.36737	0.46524

As expected, the variance of the single frequency solution was higher than variance of the dual frequency solution. The low precision errors are usually higher than one order of magnitude higher than the high precision errors. The errors are highly correlated with higher variances which can be seen more clearly in the single frequency solution.

The primary difference between the single frequency and dual frequency algorithms is how long it takes to converge to a high precision solution. This difference in solutions can be quantified by calculating the time to first fix (TTFF) which is the time needed to fix floating point ambiguities into integers. For this data set, the TTFF for the dual frequency

was roughly 2 seconds which is 4 measurement updates, and the single frequency TTFF was approximately 17 seconds which is 34 measurement updates.

Another data set was collected involving two vehicles in a dynamic convoying configuration at the Auburn RV fields. The purpose of this data collection was to determine the performance of the single frequency DRTK algorithm compared to the dual frequency algorithm in a dynamic scenario. This comparison was conducted using the dual frequency DRTK solution as the reference due to the high fidelity and accuracy of the dual frequency solution seen in previous experiments. The Novatel GPS antennas were attached to the roof of each vehicle along with the Novatel ProPak receiver. The path traveled for this data set can be seen by the GPS reported positions shown in Figure 2.4. The background mapping was made available by *GPS Visualizer*.

Figure 2.4: Novatel Reported Positions at RV fields

The azimuth and elevation of the 10 visible satellites for the data run can be seen in sky plot shown in Figure 2.5. A radio link was setup to pass measurements from the lead vehicle to the following vehicle to record the data on the computer in the following vehicle. The comparison of the algorithm solutions for this dynamic data set is seen in Figure 2.6. It is seen in the figure that the two vehicles were static for the first five minutes and for the last

minute of the data run. Using the dual frequency high precision solution as the reference, the RPV error between the two vehicles can be seen in Figure 2.7.

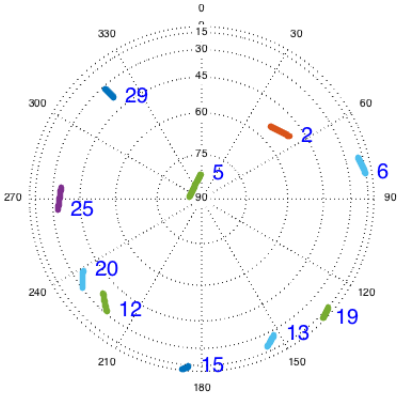

Figure 2.5: Azimuth and Elevation of Visible Satellites for a Dynamic Data Set

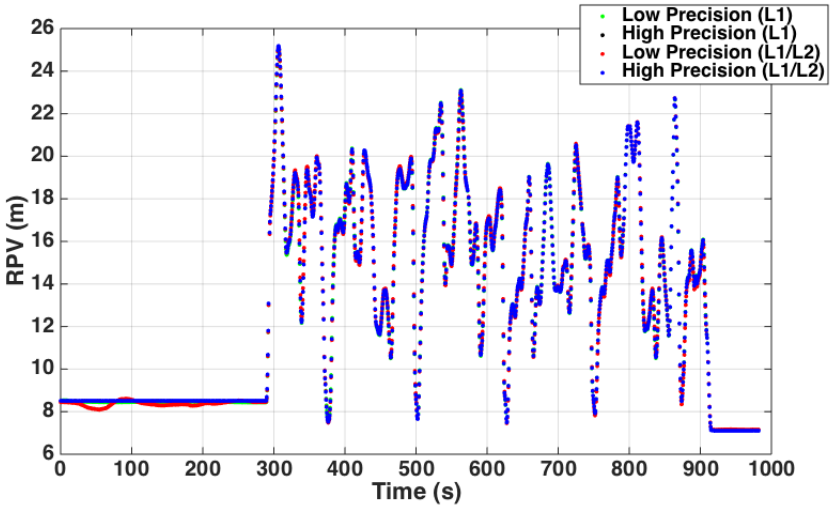

Figure 2.6: RPV for a Dynamic Data Set with Single and Dual Frequency Algorithms

It is is clear from the figures that the single frequency DRTK algorithm's performance is very similar to that of the dual frequency algorithm when the high precision solution is available. The maximum baseline error of the single frequency high precision solution compared to the dual frequency high precision solution is less than one centimeter for the duration of the data run. Even the single frequency low precision solution is more precise than the GPS reported baseline solution, which is the difference in the two GPS receiver

position solutions. Although the GPS reported baseline solution is sub-meter accurate, it is still significantly less accurate than the DRTK solutions.

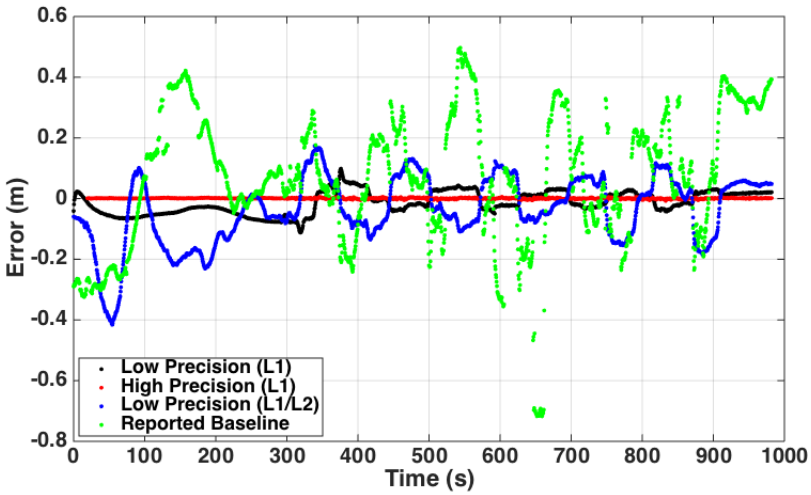

Figure 2.7: Baseline Error for a Dynamic Data Set with Single and Dual Frequency Algorithms

For this dynamic data run, the first fix for the dual frequency high precision solution occurred after the first epoch. The single frequency high precision solution's TTFF was approximately 19.5 seconds. Although the TTFF of the single frequency high precision solution is longer than the TTFF of the dual frequency solution, the accuracy is substantially better than the reported baseline solution that the receiver reports as seen in Figure 2.7.

2.11 Conclusions

Dual frequency and single frequency DRTK algorithms were provided with both high precision and low precision solutions in this chapter. These algorithms were tested to determine the fidelity and accuracy of each of the solutions. Both the high precision and low precision solutions for each of the algorithms performed better than the standalone GPS reported baseline solution. For both the dual frequency and single frequency algorithms, the high precision solution errors were primarily less than one centimeter. Because the DRTK

algorithm's residual errors are correlated with the RTK reference solution residual errors, the performance of the solution may be optimistic.

Because the single frequency algorithm's performance was comparable to the dual frequency algorithm's performance, the single frequency algorithm serves as an effective supplement depending on the system requisites.The TTFF for the dual frequency was usually just a couple epochs whereas the single frequency usually took 15-20 seconds to converge to a fix solution. The time to convergence is longer than the dual frequency and is still a limitation of the single frequency algorithm. Therefore, the TTFF proved to be the primary difference between the single frequency and dual frequency solutions.

Therefore, with given time to fix the ambiguities to integers and a good GPS environment, the single frequency DRTK algorithm is a suitable replacement for the dual frequency algorithm. However, in a poor GPS environment with little time to acquire a fixed solution, the dual frequency DRTK algorithm should be considered for implementation to ensure an accurate solution in a short period of time. Alternatively, a single frequency GPS system could be integrated with another sensor in order to achieve the reliability and precision required in vehicle to vehicle communication. One such sensor that can be utilized is a radar. Radar measurements are often used in vehicle navigation and are discussed in the next chapter.

Chapter 3

Radar Navigation and Target Selection

Other than some execptions, most autonomous vehicle following depends on line of site to the lead vehicle because many automated systems rely on vision with camera, lidar, radar, or a combination of the three [6]. In Chapter 2, it was shown how GPS measurements can be used to calculate highly accurate relative positioning information between two vehicles. However, it is well known that GPS solutions are not always available and accurate due to many of the possible errors in the GPS signal discussed in Chapter 2. Therefore, it would be advantageous to utilize other sensors in the navigation system. In this chapter, radar measurements and target selection methods are discussed along with experimentation and a performance analysis of the algorithms. For a brief summary on the history and background of Radio Detection and Ranging (radar), see [10]. In this thesis, the radar measurements and how they are used is discussed at a high-level. There has been much research in the lower-level schemes of radar navigation. However, these methods will not be addressed in this thesis. During experimentation, the radar was mounted to the front of the following vehicle in a fixed position. However, work has been done in the field of radar navigation using rotating range sensors for radar-only localization [26].

3.1 Radar Measurements

There are many different types of radars that can be used in collision-avoidance, Adaptive Cruise Control (ACC), or other ground vehicle navigational applications. In this thesis, a Delphi Electronically Scanning Radar (ESR) is used to provide range, range rate, and

bearing measurements between the following vehicle and the lead vehicle. Some of the specifications for the radar used in this work can be seen in Table 3.1 where FOV designates Field of View.

Table 3.1: Delphi ESR Specifications

Parameter	Value
Max Range	174 (m)
Mid Range	60 (m)
Accuracy: Range	0.5 (m)
Accuracy: Range Rate	0.12 (m/s)
Accuracy: Angle	0.5 (°)
Update Rate	50 (ms)
Long-Range FOV	+/- 10 (°)
Mid-Range FOV	+/- 45 (°)
Vertical FOV	4.2-4.75 (°)
Tracking Targets	64

Various types of radar will report different measurement messages depending on the specific model. These messages can include range, range rate, bearing angle, elevation angle, track status, and more. In order to keep costs low, the Delphi ESR was utilized in this work. This specific radar reports range, range rate, track status, and bearing angle. In aerial vehicle navigation, the elevation angle, not provided by the Delphi ESR, would be an important measurement to have available. However, because this work is being applied to ground vehicle navigation, the elevation angle is not a required measurement.

The range, r, measurement represents the distance between the radar and an object the radar is tracking in the path of the vehicle the radar is mounted to. The range rate, $\dot{r}$, measurement, also referred to as the Doppler or radial velocity, represents the velocity along a line extending from the radar to the tracked target. The bearing angle, θ, to the radar target is a relative angle measured from the centerline of the following vehicle. The range, range rate, and bearing measurements' physical representation are shown in Figure 3.1. The track status message indicates whether a target is an invalid measurement, a new measurement on a new channel, an updated measurement, or a merged measurement. The

track status message helps to flag poor measurements, which makes it simpler to determine which channels are reporting good measurements and eliminate the ones that are not.

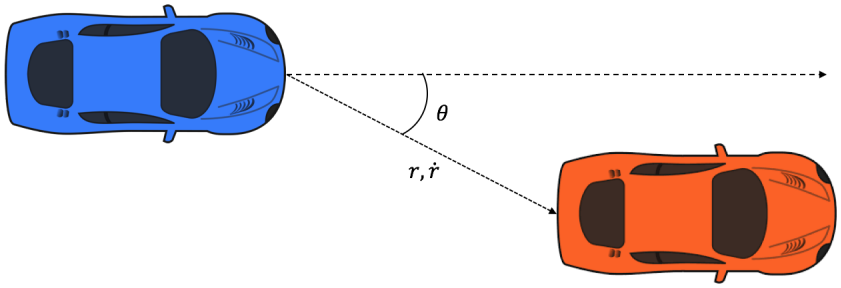

Figure 3.1: Range, Range Rate, and Bearing Measurements' Physical Representation in Convoy

3.2 Target Selection

The number of message channels in the Delphi radar is 64, which is therefore the number of targets it can track at a time as seen before in Table 3.1. This means that for every epoch, there are 64 range, range rate, and bearing measurements corresponding to 64 individually tracked targets. The process of determining which channel contains the set of measurements of the desired target from the radar is known as target selection. Because there are 64 different sets of measurements to choose from, target selection is the most complex and critical part of the radar navigation operation. In order to visualize the raw output from the Delphi radar, Figure 3.2 shows an example of the reported range measurements for all 64 channels in a given data set.

The raw output for the range rate and bearing measurements are similarly complicated and scattered. For this specific data run, the two vehicles were static approximately nine meters apart for approximately five minutes before moving. The GPS RPV solution of this data is represented by the black line in Figure 3.2.

One difficulty that occurs when using a radar to track a target is "channel jumping." "Channel jumping" occurs when the desired target leaves the FOV of the following vehicle,

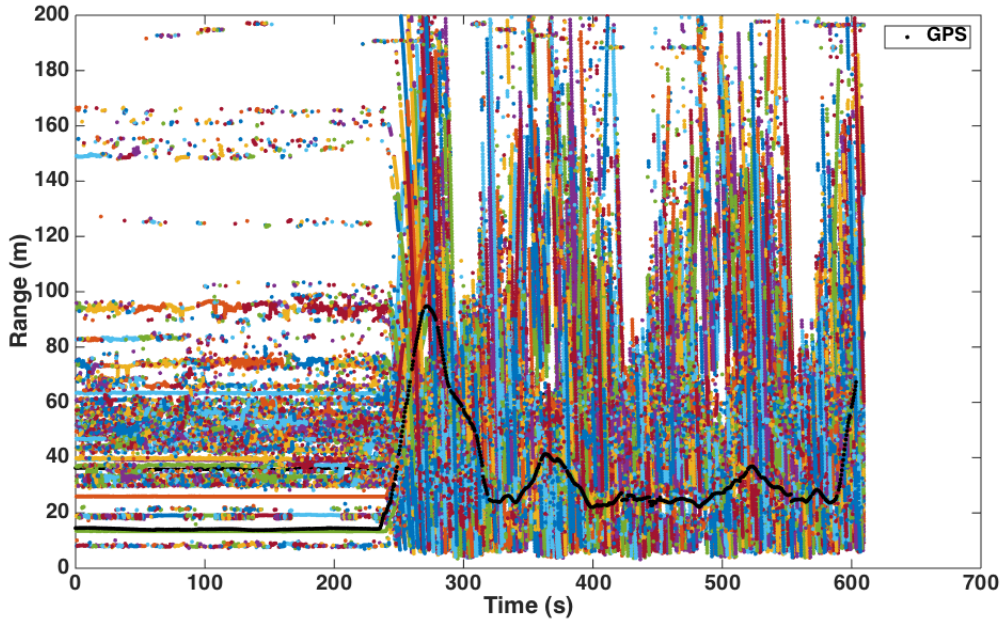

Figure 3.2: Reported Range Measurements on All 64 Channels of Delphi ESR

and there is no correct measurement reported by the radar because the radar cannot detect the desired target. Once the desired target comes back into view, the channel on which the desired target's measurements are reported has changed from the previous channel. The channel chosen out of all 64 channels is arbitrary, and therefore, the user cannot know which channel has the correct measurements once the desired target returns to the FOV. This scenario can occur when the lead vehicle enters these blind zones (outside of the FOV of the following vehicle) in tight turns or even in wide turns when the lead vehicle is far in front of the following vehicle.

The radar can also switch which channel the desired target's measurements are reported when the radar begins tracking a different part of the lead vehicle such as the opposite side of the bumper it was previously tracking. Channel jumps can also occur when other vehicles come into view or cut in between the convoying vehicles. This is a common scenario in Adaptive Cruise Control (ACC) applications where multi-vehicle target selection is important. There are many different techniques used in target selection such as lateral motion analysis, longitudinal motion analysis, in-lane target detection, and other target trajectory

estimation techniques. Many of these methods will not be addressed in this thesis but are provided in [16].

3.3 Target and Measurement Models

There are many different combinations of radar measurements to utilize in the first stage of tracking a target. In this thesis, an algorithm is developed to determine a relative position solution using radar measurements that handles the previously discussed drawbacks of radar navigation. Note that if additional information is available from other external measurements, such as an on-board Inertial Measurement Unit (IMU), these measurements can be used to better predict the change in target state. However, this would require measurements from both the lead and following vehicles. This algorithm uses the range and bearing angle measurements as measurement updates. The state vector of the radar tracker is defined below in Equation (3.1)

$$x = \begin{bmatrix} r \\ \dot{r} \\ \theta \end{bmatrix} \tag{3.1}$$

where the range is denoted by r, the range rate is designated by $\dot{r}$, and bearing angle is represented by θ.

With the assumption of a nearly constant velocity model, the target state prediction can be represented by Equation (3.2)

$$x_{k+1} = Fx_k + u_k \tag{3.2}$$

where F is a discrete transition matrix given by Equation (3.3) and u_k is a zero-mean white Gaussian process noise vector.

$$F = \begin{bmatrix} 1 & T & 0 \\ 0 & 1 & 0 \\ 0 & 0 & 1 \end{bmatrix} \tag{3.3}$$

The sampling time is denoted by T, which is 0.05 seconds in this work. The covariance matrix of the process noise vector is given by Equation (3.4)

$$Q_u = \begin{bmatrix} q_r & 0 & 0 \\ 0 & q_r & 0 \\ 0 & 0 & q_\theta \end{bmatrix} \tag{3.4}$$

where q_r and q_θ are process noise intensity parameters for the range and bearing dimensions, respectively. In this thesis, q_r and q_θ are $0.1m^2$ and 0.1deg^2.

The target oriented measurement is modeled as Equation (3.5) where H is defined by Equation (3.6) and w_k is zero-mean white Gaussian with covariance defined by Equation (3.7).

$$z_k = Hx_k + w_k \tag{3.5}$$

$$H = \begin{bmatrix} 1 & 0 & 0 \\ 0 & 0 & 1 \end{bmatrix} \tag{3.6}$$

$$R = \begin{bmatrix} \sigma_r^2 & 0 \\ 0 & \sigma_\theta^2 \end{bmatrix} \tag{3.7}$$

The target oriented measurement consists of noise corrupted range and bearing. It is important to note that there is a possibility of false measurements reported from the radar. Therefore, it is important to effectively determine which measurements should be used in the navigation solution.

3.4 Probabilistic Data Association Filter

One challenge when tracking a desired target using a radar is estimating a navigation solutoin with measurement origin uncertainty meaning that the radar reports a range measurement on a certain channel, but the user does not know what object (origin of that measurement) the radar is tracking. One way of dealing with uncertainty in the estimation algorithm is by using a probabilistic data association filter (PDAF). The PDAF approximates a mixture of Gaussian probability density functions making up the posterior state probability function. The approximation is a single Gaussian density having the same mean and covariance as the mixture. Therefore, after each scan, the estimate is built upon a Gaussian predicted density and then converted to a Gaussian mixture posterior, which is then converted back to a single Gaussian for the next scan. The PDAF is discussed in greater detail in this chapter, but for further background and examples of the PDAF algorithm, see [1–3]. For other radar tracking algorithms and methods, see [20, 21].

The operation of the PDAF using the range, range rate, and bearing measurements can be summarized in six steps. The first step in the algorithm is the prediction of the target state at scan k from the previous scan $k-1$, which can be seen in Equation (3.8).

$$\hat{x}_k = F\hat{x}_{k-1} \tag{3.8}$$

The predicted measurement, z, is then calculated as seen in Equation (3.9) along with the innovation covariance, S, shown in Equation (3.10)

$$\hat{z}_k = H\hat{x}_k \tag{3.9}$$

$$S_k = HP_kH^T + R \tag{3.10}$$

where the state error covariance matrix, P_k, is defined by Equation (3.11).

$$P_k = FP_{k-1}F^T + Q_u \tag{3.11}$$

The third stage of the operation is defining a validation "gate" centered around the predicted measurement. To visualize an instance when several validated measurements occur, Figure 3.3 shows the two-dimensional validation region for a single target represented by an ellipse in the measurement space (r, θ) [1]. The measurements are designated by Z_i, and the predicted measurement at which the ellipse is centered is denoted by $\hat{Z}^1$. The ellipse's parameters are determined by the covariance matrix, S, of the innovation. The shape is elliptical based on the assumption that the error in the predicted measurement is Gaussian. For testing purposes, the validation region can also be manually set to a constant or varying set of parameters.

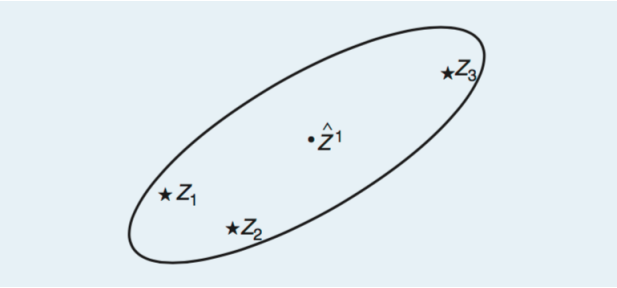

Figure 3.3: Validation Region of a Single Target with Several Validated Measurements [1]

The validation region is configured to select the measurements associated probabilistically to the target and satisfies Equation (3.12)

$$(z_k - \hat{z}_k)^T S_k^{-1} (z_k - \hat{z}_k) \leq \gamma \tag{3.12}$$

where γ determines the size of the gate. Consider a set of n_k measurements where m_k of the measurements fall within the validation region. The set form innovations are described by Equation (3.13).

$$\tilde{z}_k^j = z_k^{i_j} - \hat{z}_k, \qquad j = 1, ..., m_k \tag{3.13}$$

The next step in the algorithm is calculating association probabilities β_k^j, which represent the posterior probability that the measurement $z_k^{i_j}$ originates from the target and is defined by Equation (3.14)

$$\beta_k^j = \begin{cases} c\dfrac{1}{\sqrt{|2\pi S_k|}} e^{-[\tilde{z}_k^j]^T S_k^{-1} \tilde{z}_k^j}, & j = 1, ..., m_k \\ c\dfrac{(1 - P_D P_G) m_k}{P_D V_G}, & j = 0 \end{cases} \tag{3.14}$$

where β_k^0 is the posterior probability that all measurements at scan k originated from the previous clutter. The constant c ensures that $\Sigma_{j=0}^{m_k} \beta_k^j = 1$ (i.e., the sum of all probalilities is 100%). The probability that the target-originated measurement falls inside the validation region is denoted by P_G, which is a scalar quantity. The probability of detection is denoted by the scalar P_D. The volume of the validation gate is defined below by Equation (3.15)

$$V_G = \gamma^{n_z/2} c_{n_z} |S_k| \tag{3.15}$$

where c_{n_z} is the volume of the unit hypersphere of dimension n_z, the dimension of the measurement z_k. In this thesis, $n_z = 2$ and $c_{n_z} = \pi$ based on the work done in [21]. In a situation with no uncertainty, the probability coefficients would be unity. For this work, P_D was 0.9 and P_G was 0.95. These values are similar to those used in [1] and were selected after thorough hand-tuning of the algorithm parameters.

The next step in the algorithm is the state estimate update using the Kalman gain as seen in Equation (3.16)

$$\hat{x}_k = \hat{x}_{k-1} + K_k \tilde{z}_k \tag{3.16}$$

where K_k is the Kalman gain and is defined by Equation (3.17).

$$K_k = P_k H^T S_k^{-1} \tag{3.17}$$

The aggregate innovation is defined by Equation (3.18), which acts as a weighted average.

$$\tilde{z}_k = \sum_{j=1}^{m_k} \beta_k^j \tilde{z}_k^j \tag{3.18}$$

The next step in the algorithm is the computation of the covariance associated with the updated state as seen in Equation (3.19)

$$P_k = P_{k-1} - (1 - \beta_k^0) K_k S_k K_k^T + \tilde{P}_k \tag{3.19}$$

where the measurement dependent term, known as the "spread of the innovations," is denoted as $\tilde{P}_k$ and defined by Equation (3.20).

$$\tilde{P}_k = K_k \left[\sum_{j=1}^{m_k} \beta_k^j \tilde{z}_k^j [\tilde{z}_k^j]^T - \tilde{z}_k \tilde{z}_k^T \right] K_k^T \tag{3.20}$$

All of the previous steps relate the operation of the PDAF at a specific scan. The algorithm proceeds in a recursive manner with the same steps shown above as new measurements are received.

3.5 Experimentation and Results

In order to determine the performance of the PDAF algorithm, multiple data sets were collected and analyzed with different vehicle configurations. The location for the first data collection was at the National Center for Asphalt Technology (NCAT) test track in Auburn, Alabama. The test track, pictured in Figure 3.4, is 1.7 miles long allowing for a variety of spacing for the vehicles in convoying scenarios.

The test vehicles used in this data collection were two Peterbilt 579 trucks with trailers as seen in Figure 3.5. The following truck was equipped with a Delphi ESR which was mounted

Figure 3.4: NCAT's Test Track: Location of Data Collection

on the lower front bumper. Both the lead and following truck were outfitted with Novatel dual frequency GPS antennas and Novatel ProPak V3 GPS receivers. A radio link was setup such that the front truck could transmit GPS measurements to the following truck where the data was being recorded on a single computer. The GPS measurements were recorded in order to use the high precision dual frequency DRTK solution as a reference to test the radar algorithm's performance. The GPS measurements were also recorded in order to use the same data in the multi-sensor fusion analysis that is discussed in Chapter 4.

Figure 3.5: Test Vehicle: Peterbilt 579 Truck and Trailer

During data collection, the drivers of the test vehicles tried to maintain a constant spacing and velocity. The trucks were traveling at roughly 45 mph, a good speed to test the radar's ability to track targets and to ensure safety during testing. For each data run, the two trucks were static with the following vehicle directly behind the lead vehicle in order to initialize the radar and GPS systems.

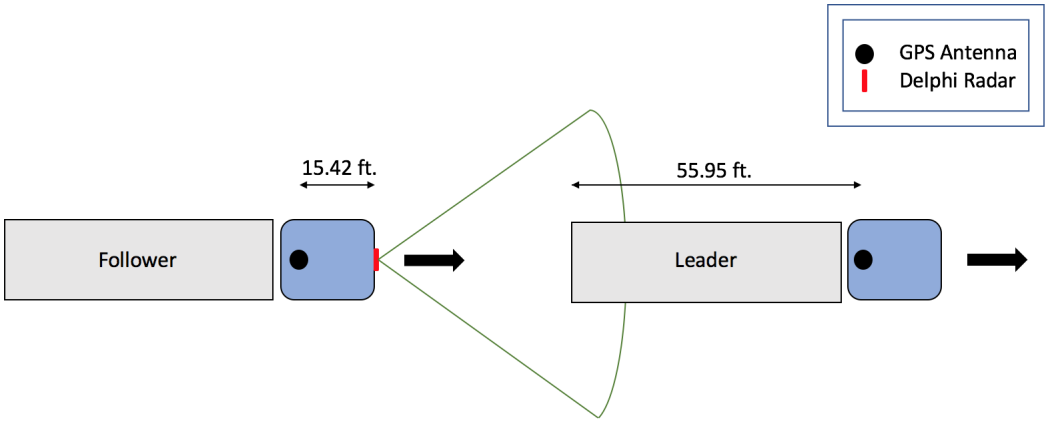

Figure 3.6: Mounting Positions of Sensors on Test Vehicles

The mounting positions of the GPS antennas and radar are shown in Figure 3.6. The two dimensions shown in Figure 3.6 sum to 71.37 feet and must be accounted for in order to accurately compare the GPS and radar solutions. Note that because the user does not know exactly what part of the rear bumper the radar is tracking, there may be discrepancies between the GPS and radar range solutions. This effect may be more evident when the vehicles are turning as the radar may be picking up a different part of the trailer on the lead truck. Therefore, the level of accuracy and consistent readings seen in the GPS solutions in Chapter 2 should not be expected from the radar's PDAF algorithm solutions.

To visualize the "channel jumping" that occurs in the radar during the data runs, Figure 3.7 shows the radar channels that contain measurements falling within the validation region in the probability association operation of the PDAF.

For all of the experimental data collections, the validation region was described by ± 10 degrees in the bearing measurement and ± 5 meters in the range measurement. These values

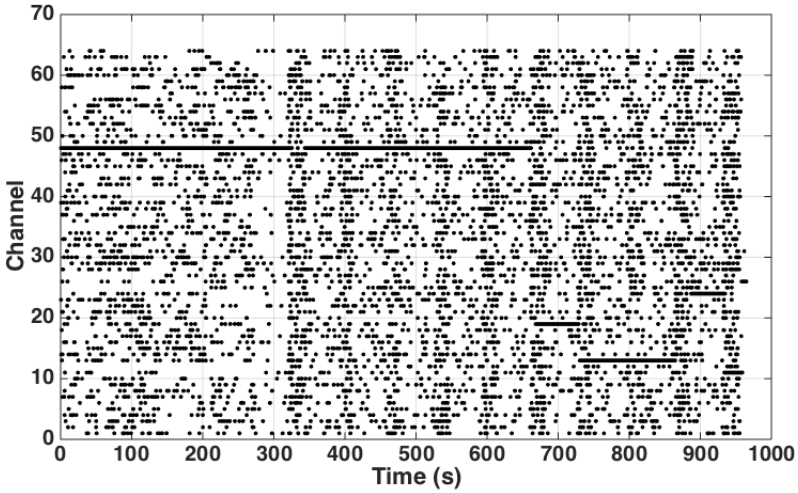

Figure 3.7: Used Radar Channels for the Trucks on NCAT Data Run

were determined after hand-tuning all the parameters and analyzing the potential dynamics that could occur inside the sample time of the measurements. In the data run, anywhere from one to seven radar channels passed the validation test to be used in the filter. Figure 3.7 shows that channel 48 in particular was one of the most consistent channels at least for the first half of the data run.

The trucks began the data set static roughly 10 meters apart for the first five minutes. The range solution between the two trucks for the radar PDAF algorithm, Novatel GPS reported baseline, and single frequency high precision DRTK solution are shown in Figure 3.8. It is evident from the figure that the single frequency high precision DRTK position solution was available for a majority of the run but not for the entire data run. The potential unavailability of the DRTK solution is one source of motivation for integrating the radar with GPS in poor GPS environments. The standalone GPS reported baseline could also be utilized when the high precision DRTK solution is unavailable. Further information on this GPS/Radar fusion is discussed in the upcoming chapters along with experimental results corresponding to the fusion system. In order to ensure that the channels that passed the validation region were from a valid target, the PDAF algorithm only accepted measurements

that passed the validation region on the same channel for five consecutive epochs. The channels used in the PDAF algorithm can be seen in Figure 3.9.

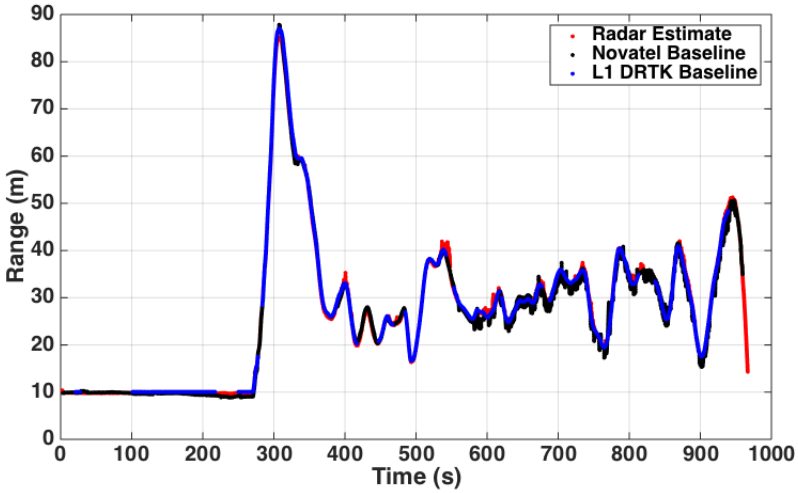

Figure 3.8: Radar, GPS Reported Baseline, and Single Frequency High Precision DRTK Range Solutions on Peterbilt Trucks at NCAT

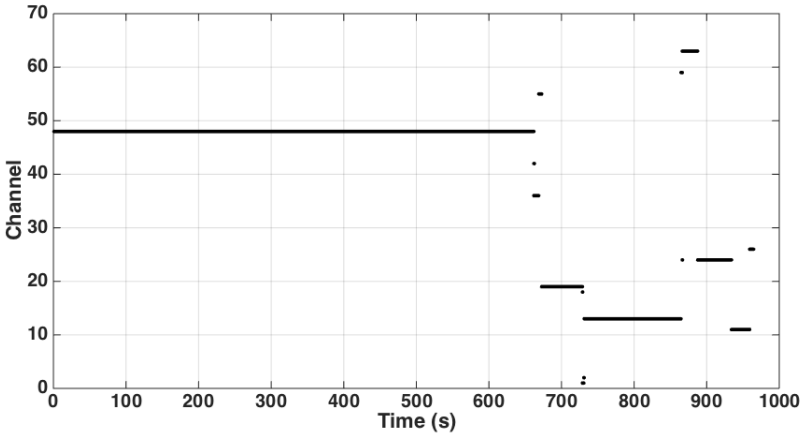

Figure 3.9: Channels Used in PDAF Algorithm for NCAT Data Run

The GPS measurements from each vehicle were synchronized using GPS time, and the radar measurements were synced with the GPS measurements using the computer's recorded time epochs. For this test, the sample rate of the Novatel GPS receivers was 10 Hz and the sample rate for the Delphi radar was 20 Hz. Due to this difference in sample rate, the GPS measurements were linearly interpolated in order to match the data rate of the radar

measurements and allow for a direct comparison of measurements. The performance of the radar PDAF algorithm solution can be compared to the single frequency high precision DRTK solution by calculating the error between the two range solutions as seen in Figure 3.10.

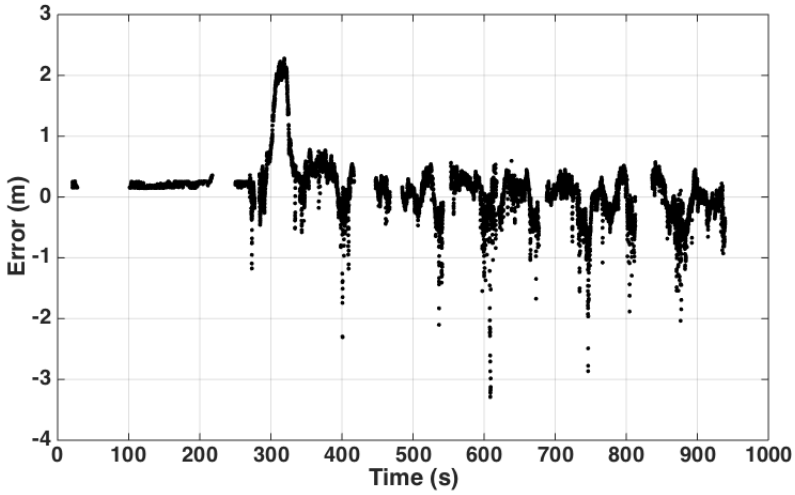

Figure 3.10: Radar Error for Data Run Using High Precision DRTK Solution as Reference with Trucks at NCAT

Figure 3.10 shows that for a majority of the data set the radar PDAF algorithm tracks the desired target reasonably well compared to the high precision DRTK range solution. The mean error for the data run is 0.3333 meters. The standard deviation of the error for the data run is approximately 0.4982 meters, which is a little higher than what would be desired for a convoying navigation solution. The highest points of error occurred while the vehicles were turning because, as mentioned earlier in this chapter, the radar may be tracking different parts of the lead vehicle's rear bumper (which is 2.59 meters wide) in the turns whereas the GPS measurements are measuring the GPS antenna positions that only vary around the true position with measurement noise. To verify this, the GPS positions of the lead and following trucks at the point in the run with the largest error are shown in a Google Maps image in Figure 3.11. All of the large errors (greater than 2 meters) in the data set were determined to have occurred in the turns using the same GPS position check.

Figure 3.11: Lead and Following Truck Positions with largest radar PDAF range error

Another source of error could be the measured dimensions of the Peterbilt truck cabs and trailers. Any errors in the measured cab or trailer dimensions of the trucks would directly bias the GPS solution and result in an inaccurate comparison of the radar PDAF range solution and the single frequency high precision DRTK range solution. Any of these errors could have attributed to the difference between the radar PDAF algorithm range solution and the high precision DRTK range solution. In this data collection, the lead truck was in the FOV of the following truck radar for the entire run.

To determine the performance of the PDAF algorithm when the lead vehicle is no longer being tracked, another data collection was completed involving a different vehicle configuration. For this set of data, the two vehicles utilized were sedans including a modified Infiniti G35 shown in Figure 3.12. The Infiniti G35 was used as the following vehicle and was outfitted with the Delphi ESR mounted on the roof right under the Novatel Pinwheel GPS antenna pictured in Figure 3.13.

The Delphi ESR was mounted on the roof of the Infiniti G35 in order to prevent damaging the front bumper while mounting the radar. Because of the height of the vehicle the

Figure 3.12: Infiniti G35 Test Vehicle Used for Data Collection

Figure 3.13: Following Vehicle Delphi ESR and Novatel Pinwheel Antenna

Figure 3.14: Lead Vehicle Novatel Pinwheel Antenna

radar was mounted, it was angled down slightly to ensure that it was tracking the bumper of the lead vehicle. The lead sedan's Novatel Pinwheel GPS antenna was mounted on the back of the trunk close to the bumper approximately where the radar would be tracking, which is shown in Figure 3.14. These mounting locations were chosen to minimize the difference in range solutions between the GPS and radar.

The location of the data collection was the RV fields off South Donahue Drive in Auburn, AL which was shown previously in Figure 2.4 and partially seen behind the Infiniti G35 in Figure 3.12. Figure 3.15 shows the radar channels used in the filter over the duration of the data run. For the first five minutes of the data run, the two sedans were parked roughly nine meters apart which is why there are primarily only two channels used in the data run as seen in Figure 3.15. Fewer channels were used in this run than in the data run with the trucks at NCAT because there were far fewer objects at the RV fields that the radar could have been tracking than at the track. At the track, the radar had multiple tracking targets on the back of the truck, which is much larger than the bumper of a sedan. After five minutes into the data run, it is evident that the desired target's radar channel changes sporadically until the end of the run. These changes mostly occur when the vehicles are turning.

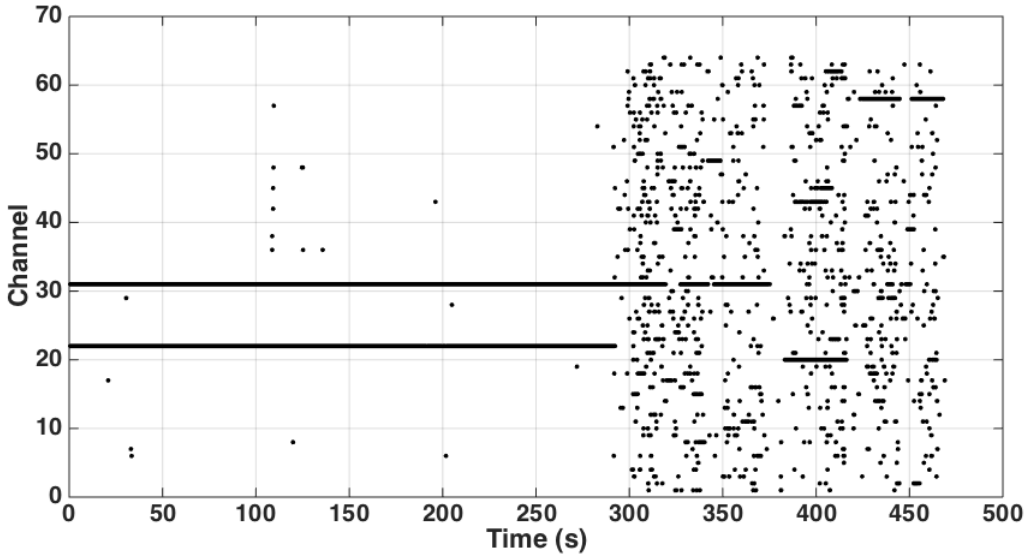

Figure 3.15: Used Radar Channels for the Sedans at RV Fields Data Run

In this data collection, there were instances when the lead vehicle left the following vehicle's FOV in sharp turns greater than 90 degrees. Some of these "blind zones" were very short, lasting as brief as a single measurement, but some of them were as long as dozens of measurements out of the FOV of the following vehicle. The radar PDAF algorithm was able to overcome some of the brief "blind zones" by relying on the estimates until a validated

measurement returned. However, in some of the larger "blind zones" the estimate drifted without any validated measurement update until the solution estimate drifted so far that no measurement could ever pass the validation gate, which was centered around the current estimate. In Chapter 4, a method of resetting the PDAF estimate using the DRTK solution will be discussed.

The standalone GPS reported baseline, single frequency high precision DRTK solution, and radar PDAF solution for the data set can be seen in Figure 3.16. Obviously, the radar PDAF algorithm estimate does not track well after about 470 seconds into the data run as seen by Figure 3.17, which shows the radar PDAF estimate error over the duration of the data run.

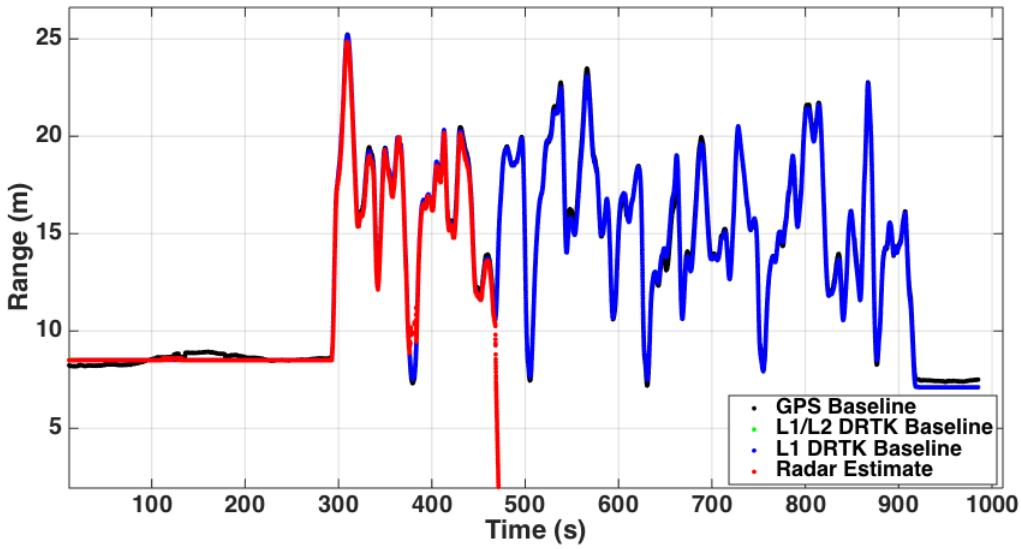

Figure 3.16: Radar, GPS Reported Baseline, and Single Frequency High Precision DRTK Range Solutions Using Infiniti G35 Test Vehicle at RV Fields

The mean error of the radar solution is centimeter-level (mean) while the PDAF algorithm is able to validate measurements. However, a very sharp turn about 380 seconds into the run was taken by the lead vehicle and the following vehicle's radar lost sight of it for several iterations. The PDAF algorithm is able to overcome this brief outage seen in the figure. Then, another "blind zone" occurs around 470 seconds into the run. However, this

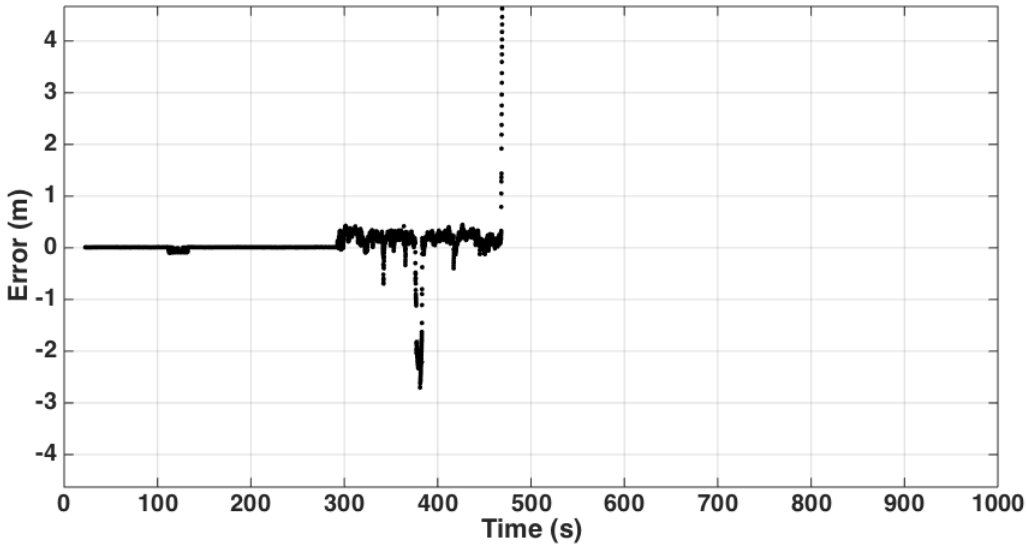

Figure 3.17: Radar Error for Data Run Using Single Frequency High Precision DRTK Solution as Reference with Infiniti G35 at RV Fields

"blind zone" is too large, and after this point in the run, the radar PDAF algorithm no longer validates measurements, which is why the radar PDAF algorithm's range solution in Figure 3.16, shown in red, drifts off. Because the algorithm knows the solution is incorrect, the system would cease reporting a solution in a real-time scenario after a whole second, or 20 epochs, without validated measurements.

It is clear in Figure 3.17 that the radar PDAF range estimate was tracking very well compared to the single frequency high precision DRTK range solution until the point in the run with the large "blind zone." The error did jump a little during the first "blind zone" but came back close to zero until approaching the large "blind zone" and drifting away. As the radar estimate drifts in this turn, the validation region in the PDAF algorithm moves along with the range estimate, away from the true value. A constant validation region would make it more difficult to adapt to unpredictable situations. If based on estimate uncertainty, the validation region can grow but can result in trusting incorrect target measurements.

These "blind zones" are a major issue in the range calculation. However, it is not reasonable to expect the radar PDAF algorithm solution to be able to maintain an accurate

estimate of the range between the vehicles if no measurements of the desired target are being reported for an extended period of time. The drift in the range solution that causes the algorithm to cease reporting a solution is induced by the algorithm holding on to the last validated Doppler measurement and predicting the next states, seen in Equation (3.8), by using the same value for $\dot{r}$ until the completion of the run. One method was investigated involving zeroing the Doppler value when no validated radar measurements were reported. This method assumes that the lead vehicle will return into view approximately the same distance from the following vehicle as it was when it left the radar's FOV, and the validation region would not move. This technique was tested and unsuccessful for these specific data sets. Another approach to investigate would be adding parameters the lead vehicle's motion to the PDAF in order to better predict the relative position of the lead vehicle.

One other possible method would be to model $\dot{r}$ as a Markov process instead of a random walk where the estimate of the Doppler would eventually level off to a constant value. Modeling this problem as a Markov process would prevent the estimate from continually drifting and cause it to settle on a constant value. However, there is no guarantee the range or Doppler between the vehicles will be the same when the desired target returns into view. Therefore, it would be beneficial to implement a multi-sensor fusion system to increase the reliability of the system. Various sensor fusion techniques are discussed in the next chapter resulting in more stable solutions.

3.6 Conclusions

A probabilistic data association filter (PDAF) algorithm was implemented for radar range estimation using the bearing and range rate measurements reported by the Delphi Electronically Scanning Radar (ESR). The PDAF algorithm was tested with various data sets to determine the accuracy and robustness of the relative position solution. The first data set that was analyzed involving two Peterbilt 579 trucks driving on the NCAT test track at a number of spacings that allowed for continuous line of sight for the radar. The

radar PDAF algorithm was successful in tracking the desired target for the duration of the run while providing an accurate range solution that was very similar to the single frequency high precision DRTK solution.

The second data set used a different vehicle setup with sharper turns that resulted in "blind zones" for the radar in which the lead vehicle was out of the FOV. Some of these "blind zones" were overcome using the PDAF estimates, but the larger ones caused the radar range estimates to drift away from truth such that the measurements tracking the desired target were no longer inside the validation region within the PDAF algorithm. The lack of validated measurements over a period of time caused the PDAF algorithm to stop reporting range solutions. Therefore, it is important to determine a method of assisting the PDAF algorithm estimation in these "blind zones" that occur when the lead vehicle is outside of the following vehicle's FOV. One option is implementing a trajectory prediction algorithm that can use various characteristics about a known vehicle to track the vehicle in the measurement clutter. An example of this work, which discusses multi-target tracking and Adaptive Cruise Control (ACC) applications can be seen in [16]. However, in this thesis, the method for solving the "blind zones" issue is by integrating another set of navigation measurements into the system in order to assist the radar PDAF solution. In the next chapter, the single frequency DRTK solution is integrated with the radar PDAF solution in a multi-sensor fusion configuration in order to acquire a more robust and precise relative positioning solution.

Chapter 4

GPS and Radar Integration for Range Determination

Next in this thesis, GPS/Radar integration is discussed and various possible configurations are evaluated to determine the best method of data fusion for relative positioning in ground vehicle applications. GPS reported positions and Dynamic Base Real-Time Kinematic (DRTK) algorithm estimates are reported at the rate of the GPS receiver which is typically less than 10 Hz. By utilizing the radar measurements in the range calculation, the relative positions can be estimated anywhere from two to five times the rate of the standalone GPS solution. This increase in update rate is vital when applying navigation solutions to convoying scenarios where faster control loops will allow for closer spacing and increased safety.

4.1 GPS/Radar Integration

Much research has been done in the area of multi-sensor fusion navigation systems including systems that integrate GPS with various sensors. These sensors can include inertial measurement units (IMU) with multi-axis gyroscopes and accelerometers, camera vision, ultra-wideband radios, lidar, and others. For examples and further details on a multi-sensor navigation algorithm using some of these sensors, see the work done in [17].

Because one of the main goals of this thesis is to develop and implement a low-cost relative positioning navigation solution, the GPS solution is integrated with the Delphi electronically scanning radar (ESR). The GPS solutions utilized in this work are the single frequency high precision DRTK range solution and the standalone GPS reported baseline such that this algorithm can operate on cheaper single frequency GPS hardware along with the low-cost Delphi ESR.

In this chapter, a few different methods of integrating GPS measurements and radar measurements are discussed. The first method implements an algorithm that utilizes the radar PDAF range solution when the desired target is being tracked (i.e., when the lead vehicle is in view) and uses the single frequency DRTK RPV solution or the standalone GPS reported baseline to update the PDAF when there is no valid radar solution. The second algorithm relies on the single frequency DRTK range solution to provide the navigation solution. If the DRTK solution is not available, then the radar PDAF solution aided by the standalone GPS reported baseline. The third technique introduced in this chapter involves a Kalman filter that fuses the DRTK and radar PDAF range solutions allowing for a higher update rate and a more reliable range solution. Each of the algorithms have benefits and limitations, and further discussion of each is discussed in the next sections.

4.2 GPS Aiding Radar PDAF

The first GPS/Radar integration method involves the radar PDAF relative positioning algorithm discussed in Chapter 3 along with the single frequency DRTK algorithm discussed in Chapter 2. This algorithm utilizes the radar PDAF range solution as long as the radar reports measurements that fall within the validation region. This means that as long as the lead vehicle is in the field of vision (FOV) of the following vehicle's radar, the algorithm will proceed with the PDAF solution. The state vector of the algorithm defined by Equation (4.1) is shown again where the r, $\dot{r}$, and θ denote the range, range rate, and bearing, respectively.

$$\hat{x} = \begin{bmatrix} r \\ \dot{r} \\ \theta \end{bmatrix} \tag{4.1}$$

The block diagram of the GPS Aiding Radar Filter (GARF) algorithm's operation can be seen in Figure 4.1. The block diagram shows that when the radar PDAF algorithm does not produce a measurement that falls within the validation region on consecutive iterations, the

single frequency DRTK solution provides the measurement update to serve as that epoch's range solution and to reinitialize the PDAF state estimate for the next epoch. In this case, the DRTK estimate of range, $\hat{r}_{DRTK}$ replaces the first term in Equation (4.1). In the case that the single frequency high precision DRTK solution is not available, the algorithm can utilize the standalone GPS reported $\hat{r}_{GPS}$ and $\hat{\dot{r}}_{GPS}$ to aid the radar PDAF algorithm.

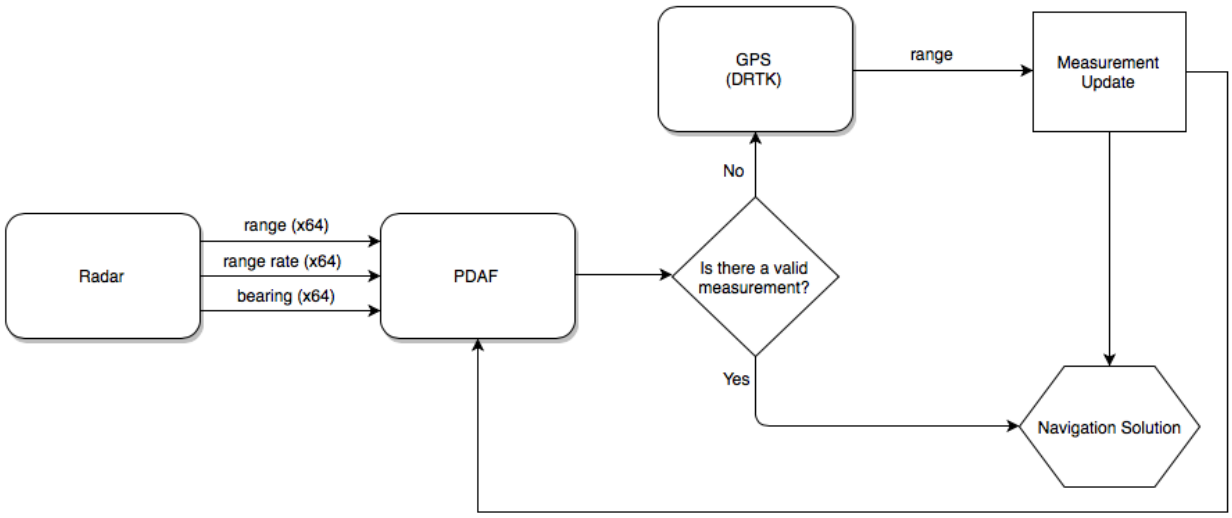

Figure 4.1: Block Diagram for GARF Algorithm

In this process, the algorithm is effectively centering the validation region of the PDAF algorithm around the single frequency high precision DRTK solution for the next set of measurements entering the system. The radar reports the next set of measurements, and the PDAF algorithm determines which measurements to validate based on the newly centered validation region. If the lead vehicle has returned to the radar's FOV, the desired target's measurement should be detected and fall inside the validation region. The radar PDAF solution will then be used until the lead vehicle is again no longer in view of the following vehicle and the single frequency high precision DRTK solution is needed to reinitialize the estimate once again.

Note that the PDAF algorithm's initial state estimate is assumed to be a priori knowledge. Because the single frequency high precision DRTK solution is not usually available at the beginning of the data runs, the standalone GPS reported baseline solution could be

used to initialize the state estimates. Experimentation and results for this algorithm are discussed in the next section.

4.3 Radar PDAF Aiding DRTK

The second method for integrating GPS and radar measurements presented in this thesis incorporates the same components as the first method but prioritizes the single frequency DRTK solution over the radar PDAF solution when a high precision solution is available. If a DRTK solution is not available, the radar PDAF range solution is utilized along with the standalone GPS reported baseline to aid the radar PDAF solution in the case that no validated radar measurements are reported. This method's performance is limited by its dependence on the single frequency high precision DRTK solution availability. However, utilizing the DRTK solution when it is available results in more accurate range estimates of the bumper to bumper spacing . The state vector for this algorithm is the same as the previous method and was shown before in Equation (4.1).

The block diagram of the Radar Aiding DRTK Filter (RADF) algorithm's operation can be seen in Figure 4.2, which shows that the DRTK solution is implemented as the navigation solution as long as it is available. For this thesis, the single frequency DRTK solution was used to accomplish the low-cost goal of this thesis. Figure 4.2 shows that if the PDAF solution does not validate any radar measurements, the standalone GPS reported baseline solution will serve as the measurement update and reinitialize the PDAF estimate as it was used in the GARF algorithm. When the radar PDAF solution does validate measurements, the PDAF range solution is used as the navigation solution for the system. The range solution will ultimately return to the single frequency high precision DRTK solution when the DRTK solution becomes available.

Just like the previous method, the PDAF algorithm's state estimate is initialized with the assumption of a priori knowledge of the initial state parameters. Again, the initial state estimates can be determined using GPS measurements of range, range rate, and bearing.

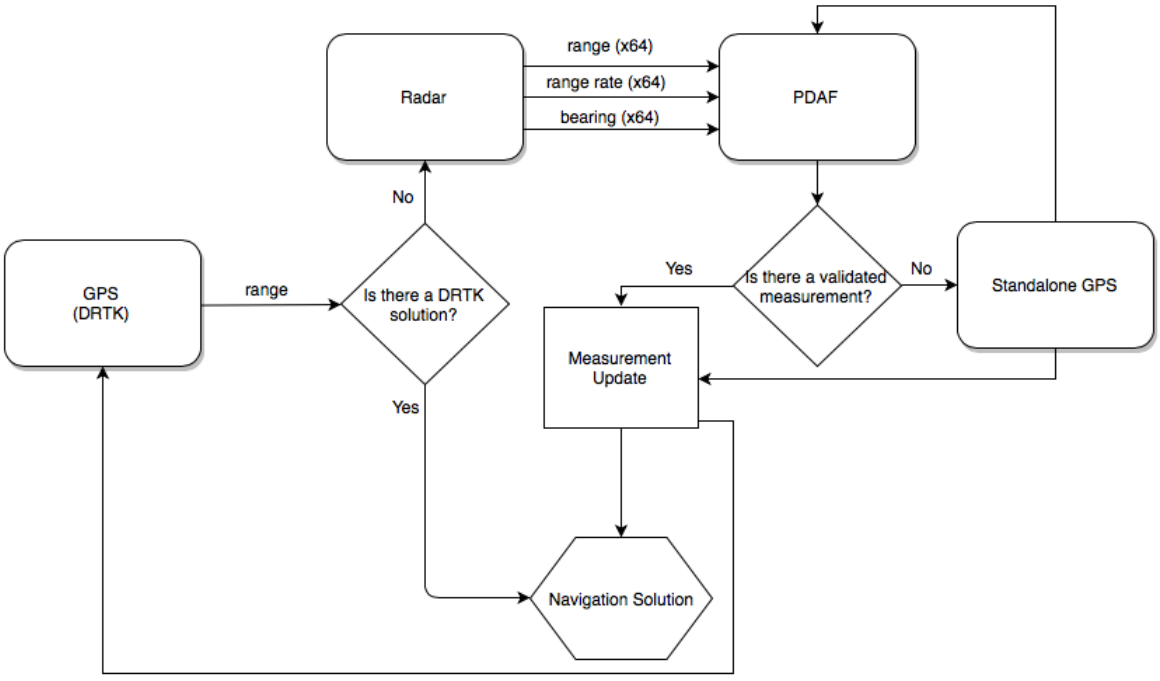

Figure 4.2: Block Diagram for RADF Algorithm

Because the single frequency high precision DRTK solution does not become fixed until several epochs into the data run as discussed in Chapter 2, the initial state estimates can be determined using the standalone GPS reported baseline solution.

4.4 DRTK/PDAF Fusion Algorithm

While the previous two methods described utilize both the radar measurements and the GPS measurements in the ranging solution, neither technique performs a direct fusion of the two sensors' measurements. Also, the difference in update rates between the GPS and radar systems limits the output rate of the RADF algorithm. If the DRTK solution was required to assist the radar PDAF system, the updates would only occur at a rate of 1 Hz or 2 Hz, which is the usually update rate for low-end GPS receivers. One second or half a second is a large amount of time when attempting close proximity convoying. An automotive vehicle control system would require a much faster update rate than what the GPS receiver could provide. Therefore, it is imperative that the DRTK solution is "interpolated" with the radar

solution in a separate Kalman Filter that combines the radar PDAF and single frequency high precision DRTK solutions.

The block diagram for DRTK/PDAF (DPKF) algorithm can be seen in Figure 4.3,

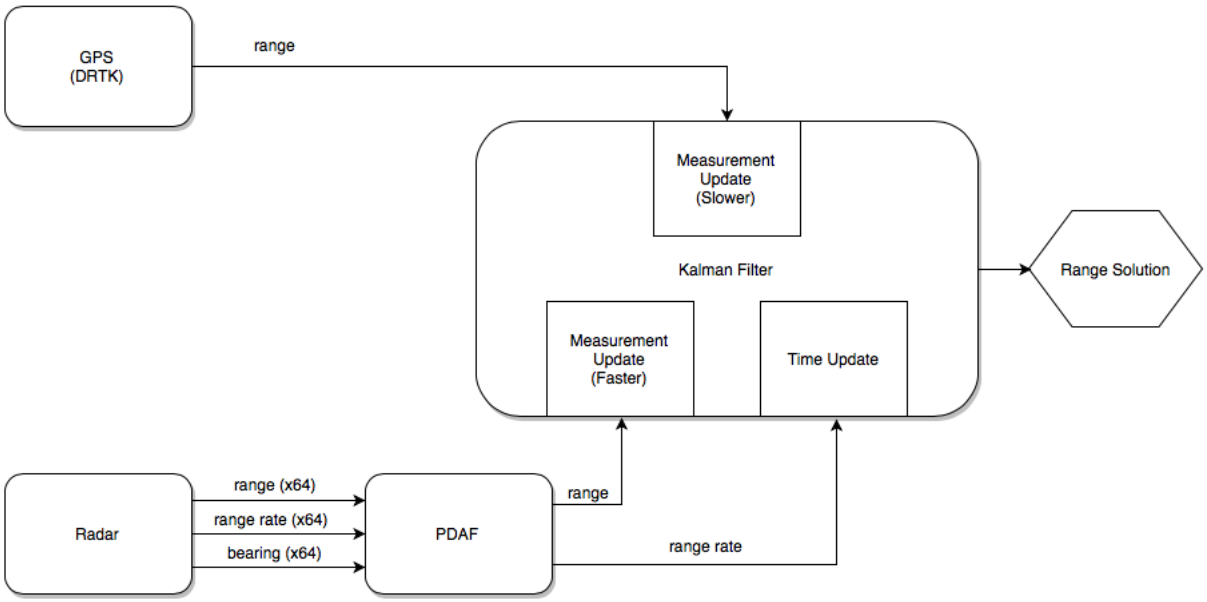

Figure 4.3: Block Diagram for DPKF Algorithm

which shows that both the DRTK and radar PDAF solutions are used as measurement updates at their individual update rates. The algorithm is a single state system that uses range, r, as the state estimate with covariance, P. The time update for the scalar Kalman filter is described by Equations (4.2-4.3)

$$\hat{x}_{k+1} = \hat{x}_k + \delta t \dot{r}_{PDAF_k} \tag{4.2}$$

$$P_{k+1} = P_k + Q \tag{4.3}$$

where δt denotes the time between updates, which for the Delphi radar in this thesis is 0.05 seconds (20 Hz), and $\dot{r}_{PDAF}$ denotes the range rate estimate output from the radar PDAF solution. The discrete covariance matrix of the process noise is represented by Q. In this thesis, $(0.01m)^2$ was used for Q based upon the resolution and variance of the Delphi ESR range rate measurements.

The measurement update consists of two updates due to the different update rates of the DRTK and radar measurements. The system update consists of two different Kalman gains and measurement covariance values for the radar and DRTK measurements. The measurement update for the PDAF measurements is described by Equations (4.4-4.6)

$$K_{R_k} = \frac{P_k^-}{P_k^- + R_{R_k}} \tag{4.4}$$

$$P_k^+ = (1 - K_{R_k})P_k^- \tag{4.5}$$

$$\hat{x}_k^+ = \hat{x}_k^- + K_{R_k}(r_{PDAF_k} - \hat{x}_k^-) \tag{4.6}$$

where r_{PDAF_k} denotes the range output from the PDAF solution. The transition matrix, H, does not appear because it is just unity. The measurement uncertainty of the radar PDAF solution and the Kalman gain associated to it are denoted by R_R and K_R, respectively. In this thesis, R_R is $(0.1m)^2$ based upon the resolution and variance of the Delphi ESR range measurements. This measurement update using the radar PDAF outputs occurs every iteration, and the DRTK outputs are used in the next part of the measurement update at the slower update rate of the GPS receiver. The GPS measurement update operation is similar to the first part of the measurement update and can be seen in Equations (4.7-4.9)

$$K_{D_k} = \frac{P_k^-}{P_k^- + R_{D_k}} \tag{4.7}$$

$$P_k^+ = (1 - K_{D_k})P_k^- \tag{4.8}$$

$$\hat{x}_k^+ = \hat{x}_k^- + K_{D_k}(r_{DRTK_k} - \hat{x}_k^-) \tag{4.9}$$

where r_{DRTK_k} denotes the range output from the single frequency DRTK solution and the Kalman gain associated to the DRTK measurement update is represented by K_D and the measurement uncertainty of the DRTK solution is represented by R_D, which is $1e^{-7}m$ in this thesis based upon the variance of the DRTK solution. Because the covariance of the DRTK

solutions is much lower than the covariance on the radar PDAF solutions, K_D should be consistently much larger than K_R. This algorithm continues in a recursive manner for the entirety of the data run.

The DPKF algorithm will perform the fusion of the radar PDAF solution and the DRTK algorithm solution utilizing the higher update rate of the radar measurements and the high accuracy of the DRTK solution inside a single Kalman filter. The higher update rate, as stated before, will allow for real-time robust control involving high dynamics and close spacing between vehicles in networks similar to ACC systems.

4.5 Performance Analysis of GPS/Radar Integration

In this section, the GPS/Radar fusion algorithms discussed in the previous section are evaluated using various data sets. The data sets that are analyzed in this chapter were collected using the same vehicles discussed in the previous chapters including the modified Infiniti G35 and the two Peterbilt 579 trucks. The performance of each of the algorithms is determined based on the accuracy of the range solution and on the stability of the solution. In platooning and convoying control systems, the vehicle to vehicle range estimate is the primary concern of the solution. For error analysis of the range estimates, the dual frequency high precision DRTK solution is used as the reference solution.

4.5.1 Truck Convoying Data Run

In the first data set, the two Peterbilt 579 trucks were used at Auburn's NCAT test track as described previously in Chapter 3. The path for the test run is shown in Figure 4.4 where the mapping background was provided by $GPS\,Visualizer$. This data set was used instead of the NCAT data set presented previously in order to show this data set's inconsistent single frequency DRTK high precision and the different fusion algorithm's response to the DRTK solution's unavailability.

Figure 4.4: Novatel Reported Path for Peterbilt Trucks at NCAT Test Track

As with the previous data set, the trucks sat static on the track at the beginning of the run in order to allow the radar time to consistently track the lead truck before moving. Also, the single frequency DRTK algorithm was given time to acquire a fixed integer solution before moving. The two truck's relative range over the period of the data run is shown in Figure 4.5. Four independent range solutions are shown in the figure (PDAF, Standalone GPS, dual frequency DRTK, single frequency DRTK). It is clear from Figure 4.5 that the single frequency high precision solution, shown in blue, was not available for the entire data run. It is also evident from the figure that the radar PDAF solution was able to maintain a relatively accurate range estimate compared with the dual frequency DRTK solution.

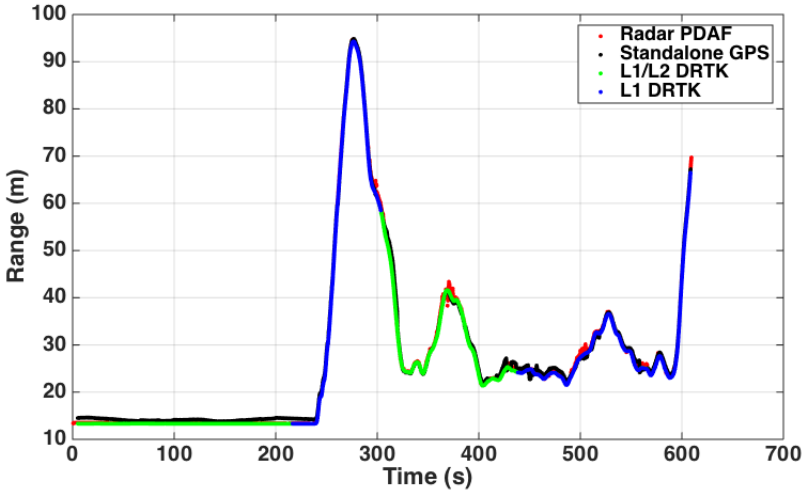

Figure 4.5: Relative Range Over Time for Data Run with Trucks at NCAT

4.5.1.1 GARF Algorithm Performance

The collected data was processed through the GPS Aiding Radar Filter (GARF) algorithm, and the resulting range error is shown in Figure 4.6. The GARF algorithm range errors were calculated using the high precision DRTK range solution as the reference. Every validated measurement solution that came from the radar PDAF is shown in red, and when no measurement could be validated in the PDAF, the standalone GPS reported baseline solution was used as the navigation solution, shown in blue. The standalone GPS solution also acted to reinitialize the PDAF estimate as described before in this chapter.

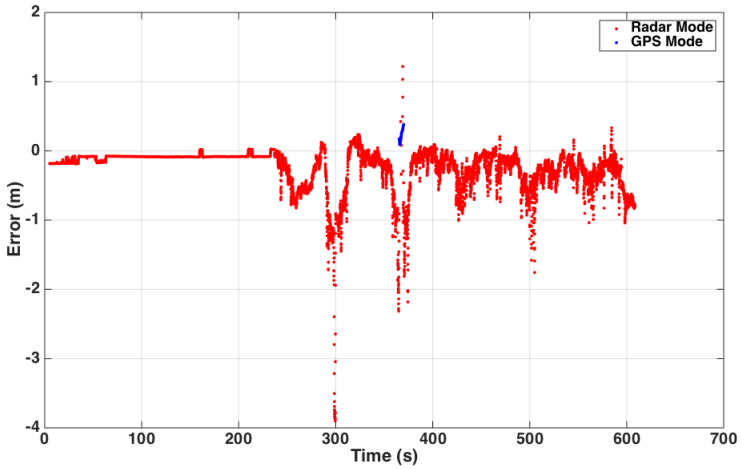

Figure 4.6: GARF Algorithm Range Error for Trucks at NCAT

Figure 4.6 shows that for a large majority of the data run, the radar PDAF solution was able to track the desired target and generate its own solution. The GPS mode can be the single frequency DRTK high precision solution or the differenced GPS baseline if the DRTK solution is unavailable. In this data set, the single frequency high precision solution was unavailable during the 300 to 400 second window. Therefore, the standalone GPS solution was utilized. The standard deviations and mean errors for the range solution in radar mode and GPS mode of the algorithm are seen in Table 4.1.

Obviously, the level of accuracy is not as high as the high precision DRTK solution. However, the algorithm's solution has sub-meter level accuracy for a majority of the run.

Table 4.1: GARF Algorithm Range Standard Deviations and Mean Error for Trucks

Mode	Standard Deviation (m)	Mean Error (m)
Radar PDAF	0.3215	0.2578
Standalone GPS	0.0885	0.2194

This level of error is not surprising considering the Delphi ESR utilized has a resolution of only 10 centimeters and the noise levels on the radar are higher than that on a GPS unit. Other factors play into the error in the solution. For instance, as mentioned previously, the radar's reported measurements may not be coming from the same exact spot on the trailer of the lead truck the entire run. The radar could be tracking the left side of the trailer and then the right side, which could change the total range between the radar and the target reported. The accuracy of the GARF solution is also dependent upon the accuracy of the dimensions of the cab and trailers of the trucks which are used to find the equivalent distance between the front bumper of the following truck and back of the lead truck's trailer. Any imperfections in the dimensions would directly create a bias in the bumper to bumper range as calculated by the dual frequency DRTK solution. This potential offset could be the cause for the 8 centimeter bias that is seen in the solution for the first 230 seconds of the data run where the trucks are sitting still. With enough data collection, this possible error source can be validated and eliminated once an accurate characterization of the bias is determined. If the mounting positions of the GPS antennas are not well known on the vehicles, then the radar solution might be trusted more than the GPS solution. Future work might consider estimating the GPS antenna offsets in real-time.

4.5.1.2 RADF Algorithm Performance

The truck data set was also processed through the Radar PDAF Aiding Filter (RADF) algorithm, and the resulting range error for this algorithm is shown in Figure 4.7. The radar PDAF solution is shown in red, the standalone GPS solution is shown in blue, and the single frequency high precision DRTK solution is shown in black. It is apparent from Figure 4.7

that for only a portion of the data run, the single frequency high precision DRTK solution was available. Between 300 and 450 seconds in the run, the DRTK solution was unavailable, and the radar PDAF solution was utilized. During that period of time, the standalone GPS solution was used for a brief period. The standard deviations and mean errors for the range solution in radar mode, GPS mode, and DRTK mode of the algorithm are seen in Table 4.2.

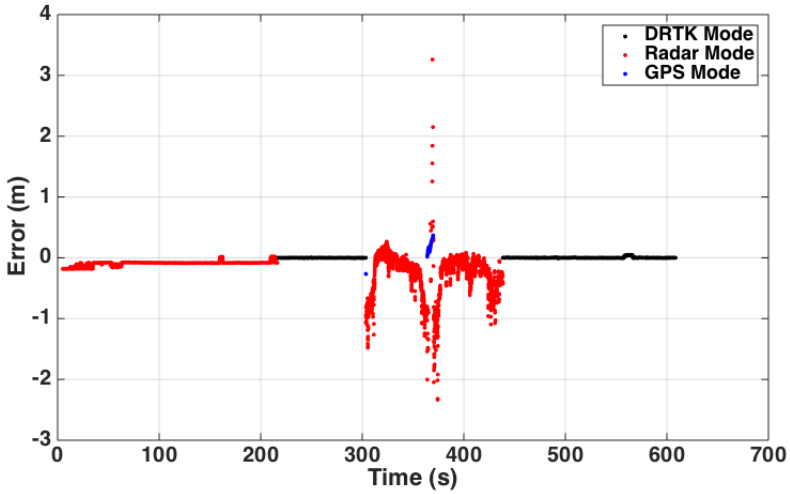

Figure 4.7: RADF Algorithm Range Error for Trucks at NCAT

Table 4.2: RADF Algorithm Range Standard Deviations and Mean Errors for Trucks

Mode	Standard Deviation (m)	Mean Error (m)
Radar PDAF	0.2542	0.1813
Standalone GPS	0.1157	0.2205
L1 DRTK	0.0075	0.0028

As expected, the accuracy of the solution was greatly improved when utilizing the high precision DRTK solution. The values seen in Table 4.2 are an improvement from the previous method. The solution is obviously more consistent when the DRTK solution is available. The single frequency DRTK solution becomes available in the data run at roughly 216 seconds, which is shortly before the trucks begin moving but still a long time for the single frequency DRTK algorithm to fix integers. However, the location was not an ideal GPS environment

due to nearby foliage and was chosen purposefully to emphasize the realistic possibilities of navigating in poor GPS environments where radar measurements can be utilized.

4.5.1.3 DPKF Algorithm Performance

The resulting range error for the truck data set processed through the DPKF algorithm is shown in Figure 4.8. The radar PDAF only solution is shown in red, the standalone GPS solution is shown in green, and the single frequency high precision DRTK solution is shown in blue. The DPKF fusion solution is shown in black.

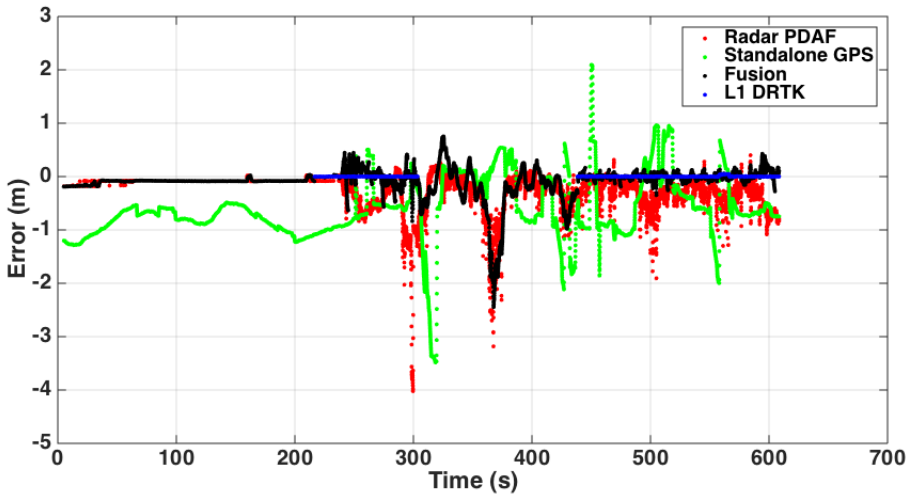

Figure 4.8: DPKF Algorithm Range Error for Trucks at NCAT

For only a couple segments of the data run, the single frequency high precision DRTK solution was available and able to assist the algorithm. Between 300 and 450 seconds in the run, the DRTK solution was unavailable and the fusion algorithm depended upon the radar PDAF solution more. During that period of time, the standalone GPS solution could have been used as a replacement for the DRTK solution. However, the mean error of the standalone GPS range solution was higher than the radar PDAF solution in a majority of the data sets collected in this research. Based upon this trend, the standalone GPS range solution was not utilized in the algorithm. However, the standalone GPS solution would be used if the radar PDAF and DRTK solutions were unavailable. Naturally, the range solution

varied much more when the high precision DRTK solution dropped out. However, the DPKF solution did maintain a reasonable level of accuracy and converged back toward the DRTK solution when the high precision DRTK solution returned. The standard deviations and mean errors for the range solution of the DPKF algorithm compared to the other solutions can be seen in Table 4.3.

Table 4.3: DPKF Algorithm Range Standard Deviations and Mean Errors for Trucks

Solution	Standard Deviation (m)	Mean Error (m)
Radar PDAF	0.3479	0.2666
Standalone GPS	0.6057	0.7390
L1 DRTK	0.0075	0.0028
DPKF	0.2830	0.1531

4.5.2 Sedan Convoying Data Run

In order to further compare the performance of the two algorithms, another data set was analyzed. This data was the same data collected using the modified Infiniti G35 test vehicle at the Auburn RV fields analyzed in Chapter 3. This data set was explored in the comparison of the algorithms because there are multiple instances when the radar loses sight of the lead vehicle and the radar PDAF estimate stops reporting a solution. Also, different test vehicles were used such that a comparison of test vehicles and environment could be made between the two data runs.

The two sedan's relative range over the period of the data run is shown in Figure 4.9. It is evident from Figure 4.9 that the single frequency high precision solution was available for a large majority of the data run. It is also clear from the figure that the radar PDAF solution was not able to maintain a relatively accurate range estimate and drifted away from the true range linearly as discussed before in Chapter 3. However, the radar PDAF estimate's absence can be aided by the algorithms developed in this chapter as will be shown in the following sections.

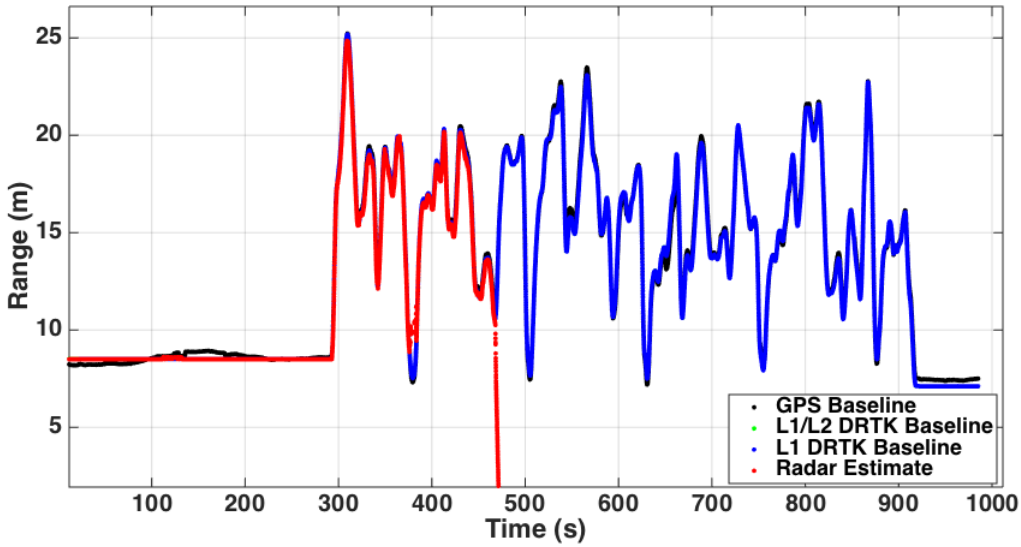

Figure 4.9: Relative Range Over Time for Data Run with Sedans at RV Fields

4.5.2.1 GARF Algorithm Performance

This second set of data was processed through the GARF algorithm, and the resulting range error is shown in Figure 4.10. The radar PDAF validated measurement solution is shown in red, and the standalone GPS reported baseline solution is shown in blue. As before, the standalone GPS solution also acted to reinitialize the PDAF estimate.

Obviously, the radar mode solution of the GARF algorithm was consistently more accurate than the standalone radar PDAF estimate due to the standalone GPS reported baseline solution aiding the PDAF algorithm when no validated radar measurements were reported. Recall that the PDAF only solution was able to overcome losing track of the lead vehicle around 380 seconds but not at approximately 470 seconds in a larger "blind zone." This larger "blind zone" was overcome using the GARF algorithm. However, later in the run, there was a spike in the error that was caused by a loss of lock in the radar that resulted in a drift of the solution as the radar locked onto another object like a telephone pole that was in the proximity of the path the vehicles were traveling. This target jump occurred in the middle of a turn at a low speed when the PDAF algorithm did not detect a large difference in velocity between the pole and the vehicle. The solution came back to the correct solution

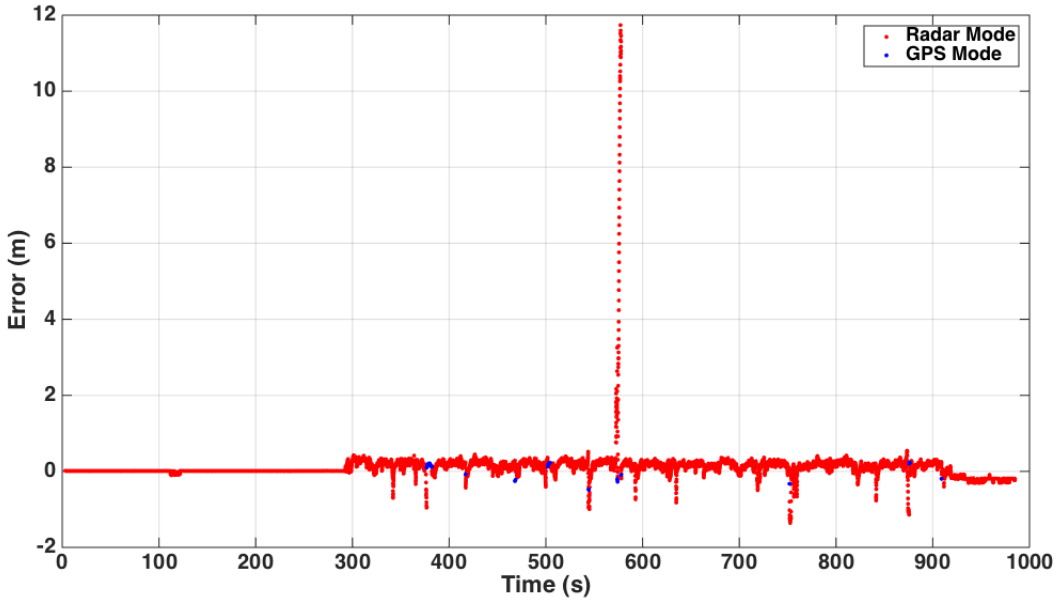

Figure 4.10: GARF Algorithm Range Error for Sedans at RV Fields

when the DRTK algorithm corrected the PDAF drift by re-centering the PDAF validation region around the DRTK range solution. The different modes' standard deviations and mean errors can be seen in Table 4.4.

Table 4.4: GARF Algorithm Range Standard Deviations and Mean Errors for Sedans

Mode	Standard Deviation (m)	Mean Error (m)
Radar PDAF	0.4943	0.1638
Standalone GPS	0.1683	0.1948

Something else worth noting is the much lower error seen at the beginning of the run where the sedans were static compared to the beginning of the previous data run with the trucks. This decrease in error was caused by the size of the target being tracked or the environment in which the data was collected. The sedan's bumper is a much smaller area for the radar to track compared to the trailer of the truck where the radar readings may have been scattered. The smaller the area, the less the data would be scattered making it more consistent. Also, there were no dimensions to incorrectly measure in order to relate the GPS range and radar range since the sensors were mounted in approximately the same location

on each vehicle as previously discussed in Chapter 3. This would eliminate the potential bias error caused by incorrect vehicle dimensions discussed earlier in this chapter.

4.5.2.2 RADF Algorithm Performance

The second data set was also processed through the RADF algorithm, and the resulting range error for this algorithm is shown in Figure 4.11. The figure shows that for only approximately 23 seconds, the single frequency high precision DRTK solution was unavailable. After that point in the run, the DRTK solution was available and used as the navigation solution for the algorithm. The standard deviations and mean errors for the range solution in radar mode and DRTK mode of the algorithm are seen in Table 4.5. The standalone GPS reported baseline solution was never required, and therefore, no error was calculated for the GPS reported baseline solution.

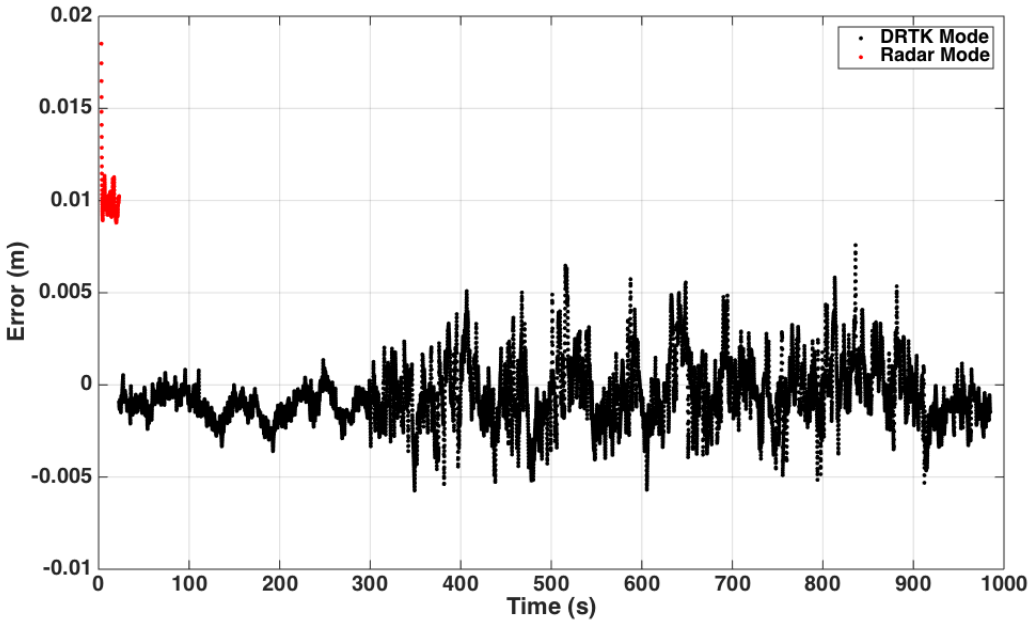

Figure 4.11: RADF Algorithm Range Error for Sedans at RV Fields

As expected, the accuracy of the solution was significantly improved when utilizing the high precision DRTK solution. The values seen in Table 4.5 are an improvement from the previous method. The solution is obviously more consistent because the DRTK solution was

Table 4.5: RADF Algorithm Range Standard Deviations and Mean Errors for Sedans

Mode	Standard Deviation (m)	Mean Error (m)
Radar PDAF	0.0100	0.0100
L1 DRTK	0.0016	0.0014

available for almost the entire data set. The single frequency DRTK solution becomes available much faster than the convergence time in the truck data set. This shorter convergence time could have been due to location which was a much better GPS environment due to continuous and good sky visibility and practically no foliage near the vehicles during the data run. The error values for the radar PDAF mode are extremely small because the radar PDAF mode was only utilized for a brief period at the beginning of the run until the single frequency DRTK solution acquired a fix.

4.5.2.3 DPKF Algorithm Performance

The sedan convoy data set was also processed through the DPKF algorithm, and the resulting range error for this algorithm is shown in Figure 4.12. As expected, the accuracy of the solution was significantly improved when utilizing the high precision DRTK solution. The standard deviation of the DPKF solution was approximately 19.6532 meters, which is definitely not accurate enough for convoying navigation. However, the accuracy and consistency of the fusion solution is obviously degraded by the inaccurate PDAF solution which drifts off indefinitely. Therefore, the GARF algorithm is utilized along with the DPKF algorithm to obtain a more stable solution. The GARF algorithm helps to correct the PDAF solution using the DRTK algorithm solution when no validated measurements were passed by the PDAF algorithm. The GARF algorithm solution was used as the input into the DPKF algorithm as opposed to the invalid radar PDAF solution.

Figure 4.13 shows the combined algorithm performance for the sedan convoying data set. By using the GARF algorithm solution to correct the radar PDAF solution, the user can continue to use the radar PDAF solution instead of relying solely upon the DRTK solution.

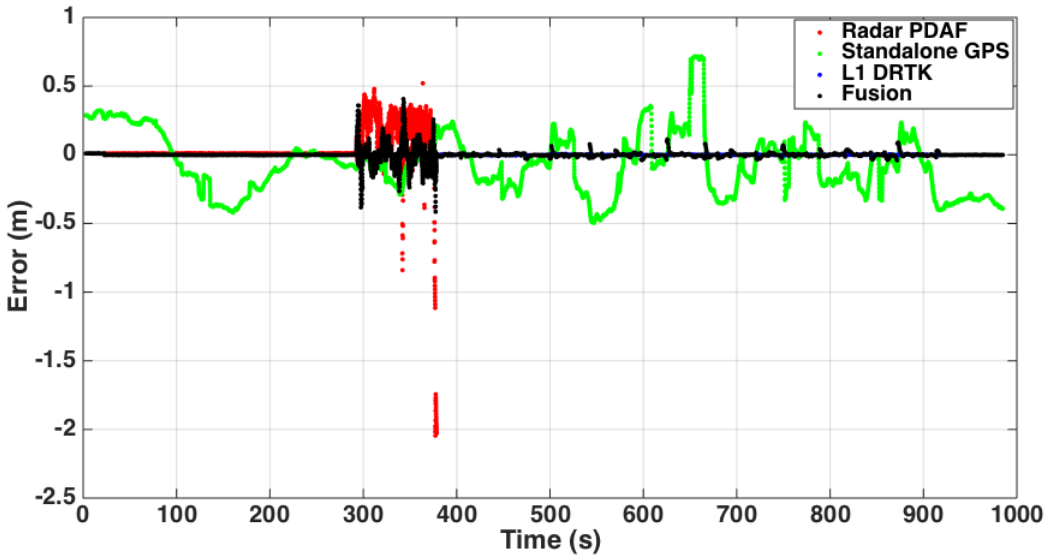

Figure 4.12: DPKF Algorithm Range Error for Sedans at RV Fields

The performance and stability of the algorithm is significantly increased when combining the GARF and DPKF algorithms. The resultant standard deviation and mean error for the combined algorithm's range solution was $0.1427m$ and $0.0452m$, respectively. This level of accuracy is expected due to the single frequency high precision DRTK solution's availability for practically the entire data run. The spike in error in the middle of the run follows the GARF algorithm's spike in error which was due to a loss of lock on the target and a drift in the solution which was corrected by the DRTK solution. The spike in error would not occur at higher speeds because the algorithm would sense a larger difference in velocities between the following vehicle and the incorrect object that the radar was tracking. Another way of diminishing the spike would be by increasing the DRTK update rate or implementing a multi-target PDAF algorithm to expect multiple targets. Wheel speed data could also be transmitted between vehicles and used to better narrow in on the speed of the target (and update) the PDAF algorithm wants to track.

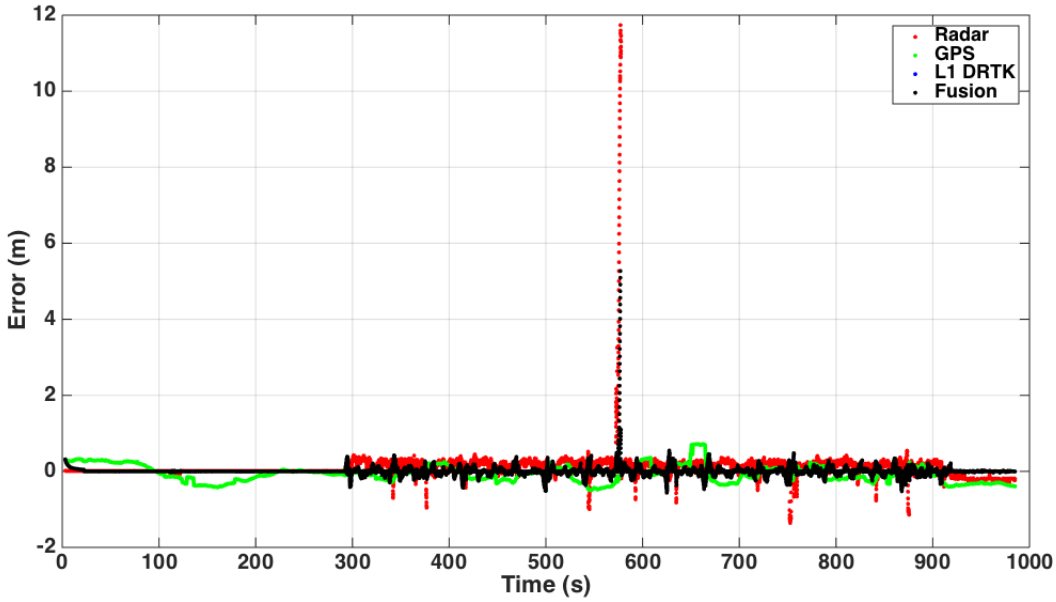

Figure 4.13: DPKF/GARF Combined Algorithm Range Error for Sedans at RV Fields

4.6 Conclusions

Three different methods for integrating GPS and radar measurements to develop a robust relative positioning navigation solution were discussed in this chapter. Also, data was collected at two locations using different vehicle configurations to test the ability of the algorithms to consistently obtain a robust relative positioning solution with reasonable precision. In these data sets, the DRTK solution was the most accurate solution due to the environment and bad target tracking, but the DRTK was not the most available solution in all the data sets. The GARF algorithm incorporated the use of the radar PDAF range solution when the lead vehicle is in the FOV of the radar. When there were no validated radar measurements, the GARF algorithm reinitialized the PDAF estimate using the GPS solution. Although the precision wasn't very high, the GARF algorithm produced a robust solution that would be very effective in low-cost implementation. The GARF algorithm requires less computational effort and is more cost-effective than other algorithms but loses the level of accuracy that DRTK can obtain.

The second method for GPS/Radar integration was the RADF algorithm that exploited the single frequency high precision DRTK navigation solution when a high-accuracy GPS fix was available. When the DRTK solution was not available, the radar PDAF range solution was deployed with the aid of the standalone GPS reported baseline solution when no radar measurements fell within the validation region. The RADF algorithm produces a more precise solution than the GARF algorithm. However, the precision of this solution is dependent on the availability of a high precision DRTK solution and requires more GPS messages to be reported and passed between the vehicles. The accuracy of the RADF algorithm is also dependent upon the accuracy of the sensor mounting position measurements on the vehicles that are subtracted from the DRTK range solution to find the effective distance from bumper to bumper. The RADF algorithm is capable of centimeter-level accuracy if a DRTK solution is available. However, more computational effort is necessary to transmit the messages required for DRTK positioning.

Finally, the DPKF algorithm incorporated both the radar PDAF solution and the DRTK range solution in a separate Kalman filter that utilized both sets of measurements in the measurement update and the range rate from the PDAF solution in the time update. The final outcome was a range solution sampled at a higher update rate with smaller variances than the radar-only PDAF solution. The DPKF algorithm performed well compared to the standalone GPS baseline and radar PDAF range solutions. The DPKF algorithm produced a much more accurate and stable range solution that is viable for low-cost, real-time applications.

The accuracy of the DPKF solution is dependent upon the accuracy of each of the measurements. One advantage of the DPKF algorithm is its ability to compute a range solution while only one of the two sensors report measurements without significant jumps in the solution. While the first two methods act more like switches between radar PDAF and DRTK solutions, the DPKF algorithm actually fuses the measurement solutions, which

allows for smoother transitions in range solutions when one of the two sensors does not report a good measurement.

Chapter 5

Conclusions and Future Work

5.1 Conclusions

Every relative positioning solutions discussed in this thesis involved GPS and radar measurements as well as different methods of determining navigation information with the measurements. The goal of this thesis was to determine the feasibility and advantages of integrating the radar measurements with the single frequency high precision DRTK range solution. Another objective of this thesis was to develop and implement a low-cost ranging system that delivered a reasonably accurate and robust relative positioning solution.

There has been substantial research in the area of multi-sensor fusion involving GPS and other sensors such as IMUs, magnetometers, and lidar. However, there was limited literature found that directly integrated GPS and radar measurements. This thesis focused specifically on utilizing the accuracy of the DRTK solution and the consistent availability of the radar measurement in environments that may not be ideal for GPS navigation.

This thesis contributed the analysis of a single frequency DRTK algorithm as well as development of a radar PDAF algorithm used to determine the correct target. Also, the analysis of the drift in the radar's range estimate when the lead vehicle left the radar's FOV was provided, which motivated the use of integrating the radar with the GPS solution. This work also contributed an analysis of different algorithms that utilize the accuracy of the DRTK algorithm along with the robustness of the radar PDAF solution using multiple vehicle configurations and environments.

At the beginning of this thesis, the various error sources that can corrupt the GPS signal, namely ionosphere delay, troposphere delay, receiver and satellite clock biases, multipath, and ephemeris error, were presented. Many of these errors can be mitigated using Differential

GPS techniques as discussed in detail in this thesis. A single frequency DRTK algorithm was developed, and the architecture for the algorithm was explained extensively. The algorithm was tested using multiple experimentally collected data sets. The experiments showed that the single frequency DRTK algorithm was capable of fixing a solution that was within a centimeter of error of the reference as long as the DRTK high precision solution was available.

It was also shown how a radar-only solution could be developed using a PDAF algorithm, assuming the lead vehicle remained in the radar FOV for the duration of the data run. The different radar measurements and errors were discussed in detail in Chapter 3. A PDAF algorithm was then developed using the Delphi ESR with experimentally collected data. The data collected was with two different vehicle configurations and environments. Depending on the following distance and path of the vehicles, the lead vehicle would stay within the FOV of the radar on the following vehicle. If the lead vehicle left the FOV of the radar, a PDAF algorithm received no accurate measurements and would drift if left in the "blind zone" for too long. As a result, the PDAF range solution was no longer reported. This issue presented motivation for using the GPS solution to reinitialize the radar PDAF estimate when no validated radar measurements were received.

Therefore, this thesis then developed a few separate algorithms that integrated GPS and radar solutions into one navigation system allowing for a more robust relative positioning solution that could also be cost-effective. The GPS Aiding Radar Filter (GARF) algorithm and the Radar Aiding DRTK Filter (RADF) algorithm both presented benefits, but both also showed limitations. The RADF algorithm delivered a more accurate range solution in the convoy scenario than the GARF algorithm. However, the RADF algorithm's accuracy is directly dependent upon the availability of the DRTK high precision solution, and the computational effort required to pass the messages over a radio link would be a disadvantage compared to the GARF algorithm. Also, the slower update rate of the GPS solution compared to the radar PDAF solution would be a disadvantage in close spacing convoying

scenarios for the RADF algorithm which utilizes the DRTK solution more than the radar solution.

Finally, a DRTK/PDAF fusion (DPKF) algorithm was developed to produce a more robust ranging solution. The DPKF algorithm allows for real-time convoy range solutions by combining the DRTK range solution with the radar PDAF solution without having to interpolate data. The faster update rate provided by the DPKF algorithm is vital for close spacing and high dynamics when controlling the system in a convoy scenario. The DPKF algorithm did show lower errors than the standalone GPS and PDAF algorithm solutions, and the DPKF algorithm solution was available for the entirety of each data set.

All of the integrated algorithms were tested using experimentally collected data sets, and the performance of each was analyzed. As expected, the RADF algorithm was more accurate when the high precision DRTK solution was available. The GARF algorithm performed reasonably well considering the quality of the radar used and the possible sources of error that could have corrupted the solution. The DPKF algorithm provided a reasonably accurate range solution at a higher update rate, but the DPKF solution did rise with the radar PDAF error spike and if not combined with the GARF algorithm, would drift back toward the invalid PDAF solution. If a higher level of accuracy is required for a specific high dynamic convoying navigation, that level of accuracy could be obtained by using a higher quality radar and by removing many of the previously discussed possible error sources. Some of these error sources could be removed by using reflective materials on the back of the lead vehicle to ensure the radar is tracking the same spot on the vehicle and confirming the dimensions of the mounting positions of the sensors on each of the vehicles are accurately measured.

5.2 Future Work

There are many steps that can be taken to further this research. It has been discussed that the radar PDAF algorithm's performance can be greatly improved by using a higher quality radar than the Delphi ESR utilized in this work. The trade-off is that the user

would be gaining a higher level of accuracy and solution stability but would be losing the cost-effectiveness of the less expensive radar system. Using a high-end radar would greatly improve the range solution. However, if the main priority is to keep the system as low cost as possible, more testing with the low-cost radar can be done to better characterize the radar. This would allow the radar PDAF algorithm's probability coefficients to be better tuned to specific values based on vehicle configuration, following distance, and path traveled. A set of radar reflectors could also be placed on the rear of the lead vehicle to potentially improve the radar's tracking of the lead vehicle. Other integration routines including a closely coupled relative DRTK/PDAF system could be considered and then compared to the system to find the most practicable integration solution for ground vehicle convoying.

The research showed that the single frequency high precision DRTK range solution had sub-centimeter accuracy compared to the dual frequency DRTK solution. However, it was apparent that the single frequency DRTK solution was not always available in poor GPS environments. Further work could be done to analyze when these outages occur in the DRTK solution and to attempt to make the single frequency algorithm consistently available. Investigation into utilizing the radar range solution to assist the single frequency DRTK algorithm in fixing integer ambiguities faster may also be worthwhile.

Another area that could be investigated in future work might be multiple target tracking with the radar and how the GPS solution could aid in determining the primary target among the various tracked targets. Previous work in literature has investigated multiple target tracking using what is known as the joint probabilistic data association filter (JPDAF). The many assumptions and the description of the operation of the JPDAF can be seen in the work done in [1]. Tracking multiple targets can be very useful in Adaptive Cruise Control (ACC) scenarios where multiple vehicles are in the FOV of the radar on the following vehicle. Some initial experimentation and description of multiple target tracking in convoying scenarios were performed in this thesis and can be found in Appendix B.

Also, investigation into target trajectory prediction could assist the radar-only PDAF solution in distinguishing the desired target among other targets. Another way of improving the radar PDAF only algorithm and the DPKF algorithm would be to incorporate an IMU or other navigation sensor into the target prediction state. With IMUs in both the lead and following vehicles, range and bearing estimates should be obtainable, and the system can "reacquire" when the lead vehicle returns to the FOV.

Also, because this thesis explored the data and the algorithms in post-processing, implementation in real-time was not investigated. However, convoying applications in leader-follower scenarios would require real-time implementation of these algorithms and methods. Transferring the algorithms currently in MATLAB code to the C++ programming language would minimize the computational effort and allow for real-time applications. The DRTK and PDAF algorithms can be computationally expansive depending on the sample rate of the data collected. However, it was performed in MATLAB with a 2 Hz update rate of the GPS receiver; therefore, real-time in C++ should be achievable. Other future work to consider would be determining the trade-off and the ideal update rate for the GPS solution to assist the radar PDAF solution (which updates at 20 Hz on the Delphi ESR).

Another issue to consider when integrating the GPS and radar solutions successfully in real-time applications is the timing of the two separate sets of sensors. The individual GPS receivers on the two convoying vehicles can be synchronized using GPS time, but the radar used in this work does not contain a GPS time stamp. Therefore, another method of time synchronization must be implemented. This might require going to a deeper level with the radar's timing system. One possible solution to this problem is using the pulse-per-second (PPS) signal from the GPS system that the radar could be synchronized with. This time synchronization would allow for better aligned measurements in the real-time integration of the GPS and radar solutions in order to use the work in this thesis in the control system of a convoy application.

Bibliography

[1] Yaakov Bar-Shalom, Fred Daum, and Jim Huang. The probabilistic data association filter. *IEEE Control Systems*, vol. 29(6), December 2009.

[2] Yaakov Bar-Shalom and T. E. Fortmann. *Tracking and Data Association*. Academic Press, Boston, Massachesetts, 1988.

[3] Yaakov Bar-Shalom, X. Rong Li, and Thiagalingam Kirubarajan. *Estimation with Applications to Tracking and Navigation*. John Wiley and Sons, New York, 2001.

[4] Eric Broshears. Ultra-wideband radio aided carrier phase ambiguity resolution in real-time kinematic GPS relative positioning. Master's thesis, Auburn University, Auburn, Alabama, August 2013.

[5] Rober Grover Brown and Patrick Y.C. Hwang. *Introduction to Random Signals and Applied Kalman Filtering*. John Wiley and Sons, New York, 1997.

[6] Cheng Chen, Han Wang, Ng Teck Chew, J. Ibanez-Guzman, Shen Jian, and Chan Chun Wah. Target tracking and path planning for vehicle following in jungle environment. In *Control, Automation, Robotics and Vision Conference*, December 2004.

[7] Paul de Jonge and Christian Tiberius. The lambda method for integer ambiguity estimation: Implementation aspects. In *LGR-Series, No. 12*, The Netherlands, August 1996.

[8] Paul D. Groves. *Principles of GNSS, Inertial, and Multisensor Integrated Navigation Systems*. Artech House, Boston, Massachusetts, 2013.

[9] William E. Travis III. *Path Duplication Using GPS Carrier Based Relative Position for Automated Ground Vehicle Convoys*. PhD thesis, Auburn University, Auburn, Alabama, 5 2010.

[10] R.J. James. A history of radar. *IEE Review*, vol. 35(9):pages 343–349, October 1989.

[11] P. Joosten and CCJM Tiberius. Lambda: Frequently asked questions. *GPS Solutions*, vol. 6:pages 109–114 , November 2002.

[12] Elliot D. Kaplan and Christopher J. Hegarty. *Understanding GPS - Principles and Applications*. Artech House, Norwood, Massachesetts, 2006.

[13] Helena Leppakoski, Heidi Kuusniemi, and Jarmo Takala. Raim and complementary kalman filtering for gnss reliability enhancement. In *In Proc. IEEE/ION Position, Location, And Navigation Symp, pages 948-956*, Coronado, CA, April 2006.

[14] Scott Martin. Closely coupled GPS/INS relative positioning for automated vehicle convoys. Master's thesis, Auburn University, Auburn, Alabama, May 2011.

[15] Pratap Misra and Per Enge. *Global Positioning System - Signals, Measurements, and Performance*. Ganga-Jamuna Press, Lincoln, Massachesetts, 2011.

[16] Seungwuk Moon, Hyoung-Jin Kang, and Kyongsu Yi. Multi-vehicle target selection for adaptive cruise control. *Vehicle System Dynamics*, vol. 48(11):pages 1325–1343, November 2010.

[17] Taragay Oskiper, Supun Samaraskera, and Rakesh Kumar. Multi-sensor navigation algorithm using monocular camera, IMU and GPS for large scale augmented reality. In *IEEE International Symposium on Mixed and Augmented Reality 2012 Science and Technology Proceedings*, November 2012.

[18] Bradford W. Parkinson and James J. Spilker Jr. *Global Positioning System: Theory and Applications Volume I*. American Institute of Aeronautics and Astronautics, Washington, DC, 1996.

[19] Benjamin W. Remondi. Performing centimeter-level surveys in seconds with GPS carrier phase: Initial results. *Journal of the Institute of Navigation*, vol. 32:pages 386–400, 1985.

[20] Mark A. Richards, James A. Scheer, and William A. Holm. *Principles of Modern Radar: Basic Principles*. Scitech Publishing, Raleigh, North Carolina, 2010.

[21] Branko Ristic, Sanjeev Arulampalam, and Neil Gordon. *Beyond the Kalman Filter - Particle Filters For Tracking Applications*. Artech House, Norwood, Massachesetts, 2004.

[22] Ying Shijun, Chen Jimbiao, and Shi Chaojian. A data fusion algorithm for marine radar tracking. In *Intelligent Computing and Intelligent Systems*, May 2009.

[23] Peter J. G. Teunissen and Sandra Verhagen. On the foundation of the popular ratio test for GNSS ambiguity resolution. In *GNSS 17th International Technical Meeting of the Satellite Division*, Long Beach, CA, September 2004.

[24] P.J.G. Teunissen. The least-squares ambiguity decorrelation adjustment: A method for fast GPS integer ambiguity estimation. *Journal of Geodesy*, vol. 70:pages 65–82, November 1995.

[25] William E. Travis, David W. Hodo, David M. Bevly, and John Y. Hung. Ugv trailer position estimation using a dynamic base RTK system. In *AIAA Guidance, Navigation and Control Conference and Exhibit*, Honolulu, Hawaii, August 2008.

[26] Damien Vivet, Paul Cheochin, and Roland Chapuis. Radar-only localization and mapping for ground vehicle at high speed and for riverside boat. In *Robotics and Automation, IEEE International Conference*, May 2012.

Appendix A

GPS Characteristics

There are multiple steps involved in the computation of a GPS receiver's global position, which begins with an iterative least squares solution after the pseudorange observation measurements are linearized. The pseudorange, a rough range between the GPS receiver and specific satellite, is calculated by multiplying the speed of light by the travel time from the satellite to the time the signal was received. The timing of the GPS signals are discussed in the next section.

A.1 GPS Time Calculations

The determination of timing is the basis of GPS techniques. The first step is the initial calculation of the pseudorange. The traveling time between the satellite and the receiver, τ_r^s, is computed by differencing the time the signal is sent from the satellite, t^s, and the time the signal is received, t_r. This can be seen in Equation (A.1).

$$\tau_r^s = t_r - t^s \tag{A.1}$$

Then, the pseudorange, ρ_r^s, can be determined by multiplying the signal travel time by the speed of light, c. This is seen in Equation (A.2).

$$\rho_r^s = \tau_r^s * c \tag{A.2}$$

The satellite and receiver have innate clock errors that must also be modeled. The models of these errors are shown in Equations (A.3) and Equation (A.4).

$$t^s = (t_r - \tau_r^s) + dt^s \tag{A.3}$$

$$t_r = t_{GPS} + dt_r \tag{A.4}$$

The pseudorange is known as an observable in hardware receivers. Therefore, the satellite transmit time, t^s, can be calculated, and after mitigating the satellite clock error, dt^s, the transmit time can be acquired in GPS time.

A.2 Dilution of Precision

Dilution of precision (DOP), or geometric dilution of precision (GDOP), is a phrase used in satellite navigation to specify the additional multiplicative effect of satellite geometry on the precision of positional measurements. There are several different variations of the dilution of precision, including geometric (GDOP), vertical (VDOP), horizontal (HDOP), position (PDOP), and time (TDOP). The values of these are shown in Equations (A.5) - (A.9).

$$GDOP = \sqrt{\frac{\sigma_e^2 + \sigma_n^2 + \sigma_u^2 + \sigma_{cb}^2}{\sigma_0^2}} \tag{A.5}$$

$$VDOP = \frac{\sigma_u}{\sigma_0} \tag{A.6}$$

$$HDOP = \sqrt{\frac{\sigma_e^2 + \sigma_n^2}{\sigma_0^2}} \tag{A.7}$$

$$PDOP = \sqrt{\frac{\sigma_e^2 + \sigma_n^2 + \sigma_u^2}{\sigma_0^2}} \tag{A.8}$$

$$TDOP = \frac{\sigma_{cb}}{\sigma_0} \tag{A.9}$$

These DOP values are dimensionless and give rough position error when multiplied by the predicted range errors of the receivers. The magnitudes of the DOP values are determined

by the current satellite constellation. For further information on the dilution of precision and its different variations, see [15].

Appendix B

Tracking Multiple Targets and ACC Applications

In the field of driver assistance and collision avoidance technologies, there have been many developments recently. An example of this is called adaptive cruise control (ACC), which relies on radar or lidar readings and automatically adjusts the vehicles heading and speed to sustain safe following distances with vehicles in the same lane [16]. The ability to track multiple targets in a convoying scenario is imperative so that the following vehicle does not ignore a closer vehicle while tracking the lead vehicle and collide with the secondary vehicle.

In order to test the algorithm's ability to track secondary vehicles in the convoying scenario, another data set was collected using the two Peterbilt 579 trucks and the modified Infiniti G35 sedan presented in Chapter 2. The data collection took place at the NCAT test track such that both lanes of the track could be utilized for the data run. The trucks were traveling at a speed of approximately 45 miles per hour such that the Inifiniti G35 could cut in and out safely. Each truck was outfitted with a Novatel ProPak GPS receiver and Novatel antenna. The following truck held a Delphi ESR on the bottom of the front bumper.

Similarly to the previous data sets analyzed in this work, the two trucks began the data set static before beginning the run. The modified Infiniti G35 sedan came up beside the following truck, cut in front of the following truck, exited the truck's lane, and then dropped back behind the following truck. This occurred twice during the data run, which lasted roughly 8.5 minutes. Figure B.1 shows the Infiniti G35 exiting the travel lane in the multiple vehicle convoy scenario.

Much work has been done in the area of multi-target tracking using radar in recent past. A modification to the probabilistic data association filter (PDAF) tracking algorithm used in

Figure B.1: Multiple Vehicle Convoy Data Collection at NCAT Test Track

this work is known as the Joint PDAF (JPDAF). A detailed description and example of the JPDAF can be seen in the work done in [1]. In this thesis, a more straightforward technique was implemented. The GARF algorithm described in Chapter 4 was utilized during the data run. However, a set of logical conditions were implemented in order to allow the system to read and track other targets in the radar's FOV. These conditions included tracking targets that had a nonzero range rate that was under a certain threshold. The threshold used in this work was 4 meters per second due to the dynamics of the data run. This condition allows the system to track any object that is traveling within that threshold relative to the following vehicle to be tracked.

The next condition implemented involved targets that reported a smaller range measurement than the primary target (lead truck). This condition is important because closer targets are a larger concern than the farther targets when considering collision avoidance

situations. If the low range rate and smaller relative range conditions are met, the system will override the GARF algorithm's range solution and transition the primary target to the closer vehicle as long as the closer vehicle maintains those conditions. Figure B.2 shows the Delphi ESR reported range measurements on all 64 channels for the duration of the data set.

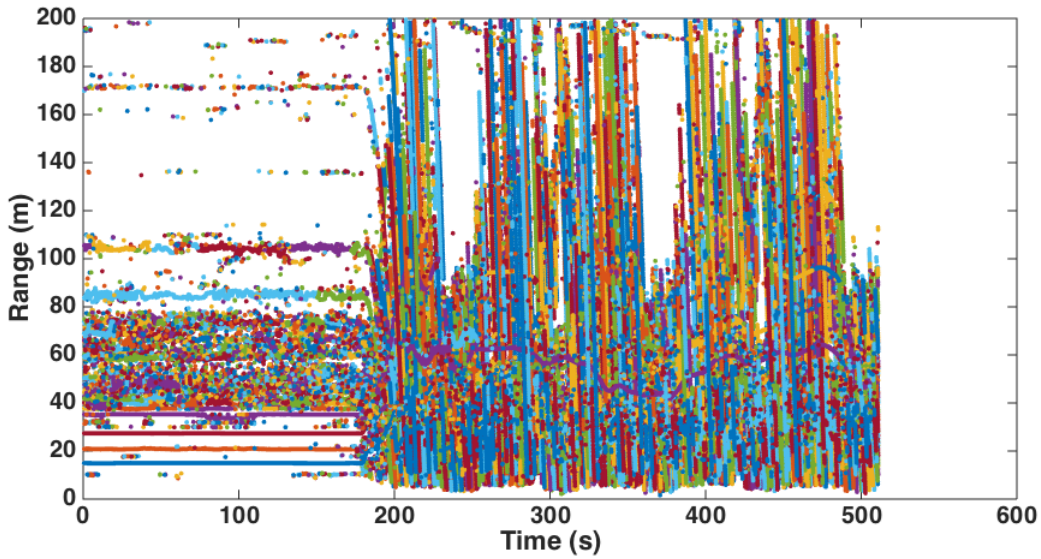

Figure B.2: Delphi ESR Reported Range Measurements for Multiple Vehicle Convoy Data Collection at NCAT Test Track

Figure B.3 shows the range solutions using the GARF algorithm, the standalone GPS baseline, and the DRTK solutions over time for the lead truck during the run. It is apparent from Figure B.3 that the Delphi ESR on the following truck was able to track the lead truck for the entirety of the data set even as the sedan cut in front of the following truck. It is assumed this was possible due to the distance between the vehicles and the height of the trailer on the lead truck. The two conditions previously mentioned involving range rate and range parameters were implemented on the data set to find which radar channels at which epochs met these stipulations. The results showed that channels 6 and 24 met these conditions for a certain period of time at two separate segments in the data run.

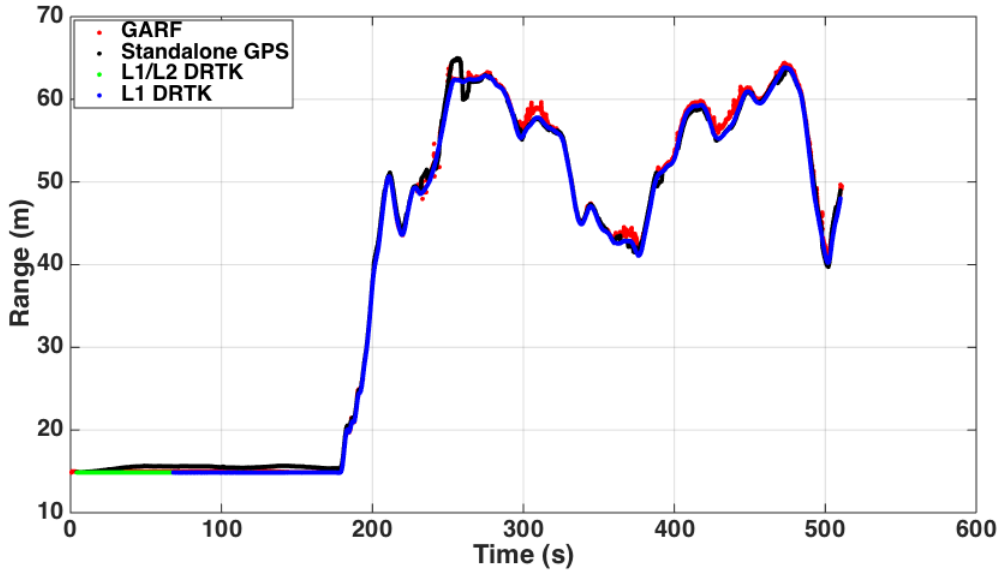

Figure B.3: Range to Lead Truck in Multiple Vehicle Convoy Data Collection at NCAT Test Track

The resultant range solutions for the multiple vehicle convoy scenario can be seen in Figure B.4. In the figure, the blue data points show the GARF algorithm solution for the lead truck over the duration of the data set. The orange shows the two instances that the Infiniti G35 cut in between the two convoying trucks. The data points shown in black around 180 seconds into the data run are data points reported from another target. Roughly 180 seconds into the run, the trucks began moving and the radar picked up a sign on the side of the track, and because the sign was closer to the truck and the following truck's speed was not very high, the conditions were met to make the sign the primary target. Once the truck increased speed, the sign's relative speed to the truck was much higher than the threshold, and the lead truck was reinstated as the primary target in the algorithm. This issue could be resolved by setting another condition that the relative range and range rate conditions are only considered when the following vehicle is moving at a high enough speed. Because the radar is only reporting a relative velocity between vehicles, another sensor is required for ground speed measurements. A wheel speed sensor or GPS velocity could be used in this scenario. The GARF algorithm is already being used to obtain the lead truck's range

solution; thus, the GPS velocity measurement would be the most reasonable measurement to use in this situation.

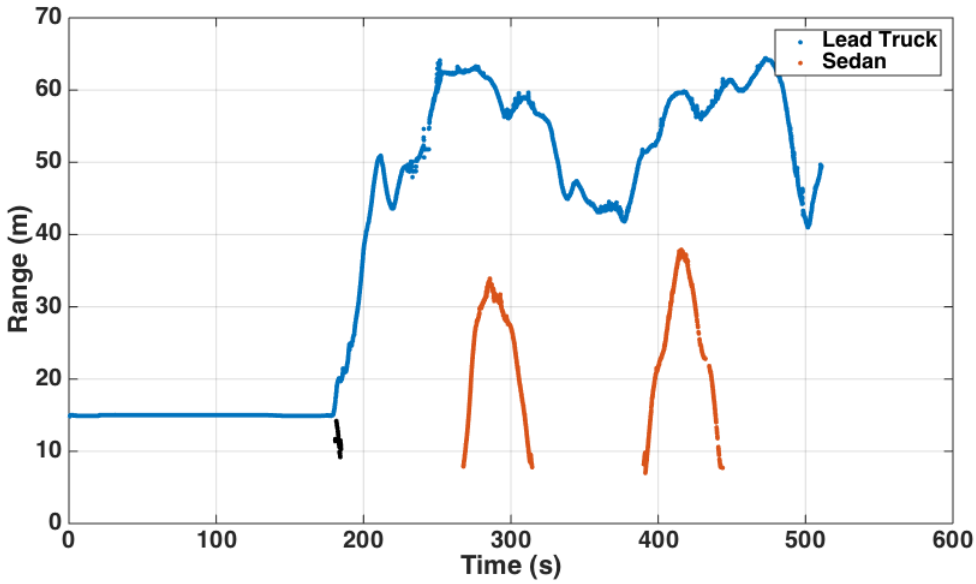

Figure B.4: Range Solutions for Lead Truck and Sedan in Multiple Vehicle Convoy Data Collection at NCAT Test Track

The method for multiple target tracking presented in this section is not as sophisticated as other techniques implemented in other works. However, setting conditions for relative range, relative range rate, and ground speed can be simple logical steps in refining a navigation solution involving multiple vehicles in a convoying scenario. For further description of multi-vehicle target selection, see the work presented in [16] and [3].